Anomalous Diffusion and Mixing of Chaotic Advection in a Rayleigh-Benard Flow

大内, 克哉
Graduate School of Sciences, Kyushu University

https://doi.org/10.11501/3075381

出版情報：九州大学, 1993, 博士（理学）, 課程博士
バージョン：
権利関係：

Anomalous Diffusion and Mixing of Chaotic Advection in a Rayleigh-Bénard Flow

大　内　克　哉

Anomalous Diffusion and Mixing of Chaotic Advection in a Rayleigh-Bénard Flow

Katsuya OUCHI

Department of Physics
Kyushu University 33,Fukuoka 812

March 1993

Contents

Abstract

Solomon and Gollub discussed a transport property of fluid particles in nearly two-dimensional, time-periodic Rayleigh-Bénard convection. They determined the diffusion constant D in terms of Fick's law by taking only short time characteristics of the trajectories. In this thesis D is defined by the variance for large time. Hence D is determined by the long time correlation of the trajectories, and several fine-grained peaks are observed in the graph of D vs the amplitude B of lateral oscillation. Accelerator-mode islands appear around the oscillating roll boundaries in a peak range of B and the formation of the islands are elucidated in terms of the lobe dynamics.

Mixing of tracer particles by chaotic advection is discussed in terms of the spectrum $\psi(\Lambda)$ and the probability density $P(\Lambda; n)$ of the coarse-grained expansion rates Λ_n. These physical quantities show an anomalous scaling due to the intermittent sticking of tracer particles to the islands. $\psi(\Lambda)$ has a linear part of slope 0, i.e., $\psi(\Lambda) = 0$ for $0 < \Lambda < \Lambda^\infty$, where Λ^∞ is the Liapunov exponent. $P(\Lambda; n)$ obeys an anomalous scaling law $P(\Lambda; n) = n^\delta p\{n^\delta(\Lambda - \Lambda^\infty)\}$ with $\delta < 1/2$, where $p(x)$ is a power law function for $-x \gg 1$. These characteristics are generic in Hamiltonian dynamical systems.

1 Introduction

The study of chaotic motions in nonlinear oscillator systems has been one of rapidly growing fields of physics for the last decades, with applications to a number of areas in science and engineering, including astronomy, plasma physics, statistical mechanics and hydrodynamics. Although the root of the fields is old, dating back to the last century when Poincaré and others attempted to formulate a theory for nonlinear perturbations of planetary orbits [1], the field progressed remarkably in the 1960's, together with computational results obtained by using high speed computers, that facilitated our new treatment of the subject. The systems, however, had been mainly concerned with conservative ones. Further in the 1970's, an another field of the chaotic properties, i.e., dissipative systems, began to progress with the discovery of strange attractors. A strange attractor was found numerically in 1963 by Lorentz [2], and the idea was elavorated mathematically in 1971 by Ruelle and Takens [3] as a key element in understanding irregular behavior described by deterministic equations, notably turbulence.

A main emphasis in both systems is the existence of sequential stretching and folding processes, which lead to the intrinsic stochasticity in the deterministic system. The processes are very important since they mediate between stochasticity and determinism. For example, when the motion of tracer particles in the Rayleigh-Bénard convection is studied below, it can be regarded as a diffusion process in spite of the fact that the equation of motion is deterministic. Such the processes lead to a mixing of particles, and

hence the mixing is one of the main themes in studying the chaotic motions.

It is often useful to regard the motion of tracer particles in hydrodynamic flows as a conservative motion. The particle is considered as a virtual particle; namely a particle with proper mass which does not affect the velocity field and which is not stirred due to the Brownian effect. The motion is determined from a velocity field $\vec{v}(\vec{r},t)$ with

$$d\vec{r}/dt = \vec{v}(\vec{r},t) \tag{1.1}$$

and is denoted as the Lagrangian representation. The kinetic equation to determine the velocity field $\vec{v}(\vec{r},t)$ is the Navier-Stokes equation, which is a well-known nonlinear partial-differential equation. Hence the behavior of the tracer particles is easily analyzed both theoretically and experimentally.

The control parameter of the equation is the Reynolds number formed from the three parameters, the velocity of the main stream, one linear dimension and the kinematic viscosity [5]. For sufficiently large Reynolds number, the velocity field is turbulent temporally and spatially, and the state is sometimes referred to as the Eulerian turbulence. The tracer particles are of course chaotic in that regime. The turbulence has been studied for a long time and much have been obtained.

Aref, on the other hand, first showed in 1984 that the tracer particles may be chaotic even in laminar flows [6], where the regime is referred to as the Lagrangian turbulence as compared with the Eulerian turbulence. The viewpoint is as follows. For two-dimensional incompressible flow, the equation for tracer particles (1.1) is formally a Hamiltonian equation with just

one degree of freedom. For unsteady flow, the system is non-autonomous and one must in general expect to observe chaotic particle motion. He developed these ideas and subseqently corroborated through the study of a very simple model which provides an idealization of a stirred tank. In the model the fluid is assumed incompressible and invicid, and its motion wholly two-dimensional. the agitator is modeled as a point vortex, which, together with its image in the bounding contour, provides a source of potential flow. The motion of a tracer particles in this model device is computed numerically. It is shown that the deciding factor for integrable or chaotic particle motion is the nature of the motion of the agitator. With the agitator held at a fixed position, integrable tracer particle motion ensures, and the model device does not stir very efficiently. If, on the other hand, the agitator is moved in such a way that the potential flow is unsteady, chaotic tracer particle motion can be produced. This leads to an efficient stirring.

These ideas are quite generic for incompressible hydrodynamical flows, and hence many other fluid systems have been studied after Aref's first work. For example, D.S.Broomhead and S.C.Ryrie studied the trajectories of individual tracer particle moving in velocity fields which model Taylor vortices close to the onset of the wavy instability [7]. In particular, they consider the possibility of transporting particles between rolling cells. By studying the flow in the context of dynamical systems theory, it is shown that this arises through the destruction of invariant surfaces which form the roll boundaries in the absence of the wave. Particles able to pass between cells follow chaotic

trajectories.

An important characteristic in studying the Lagrangian turbulence is that chaotic structures can be easily analyzed both theoretically and experimentally. Indeed, Franjione, Leong and Ottino showed experimentally that simple two-dimensional time-periodic flows produce chaotic mixing and, depending on the choice of the period, large dynamical structures called islands, that change the form in a time-periodic manner but remain segregated even after long times [8]. Since an analytic expression for the velocity field does not exist in this system, making theoretical prediction of the location and size of islands is impossible. Hence the flow is analyzed in terms of its symmetries which is obtained from the gross properties of the velocity field. With this knowledge, an island is moved into a region of good mixing in a systematic way by manipulating symmetries.

Ishii, Iwatsu, Kambe and Matsumoto studied a three-dimensional flow of viscous incompressible fluid in a cubic space with a moving upper wall by solving numerically the Navier-Stokes equation itself [9]. Steady solutions are obtained at low Reynolds numbers. It is found that the trajectories of the tracer particles exhibit complicated structures even in the steady-state flow fields. The characteristics of the trajectories are examined in detail for a wide range of the Reynolds number. At the low Reynolds numbers in the steady regime, some sets of helical trajectories form invariant tori. As the Reynolds number increases in the region, certain invariant tori are disrupted by resonances and a region of chaotic trajectories coexists with

regions of invariant surfaces. The chaotic region becomes larger in the space at higher Reynolds numbers. They ensured that the particle motion in a steady solenoidal velocity field is equivalent to a non-autonomous Hamiltonian system of one-degree-of-freedom.

In general, an onset of the Lagrangian turbulence is related to a bifurcation of the velocity field, but the onset is generally not related to the onset of the Eulerian turbulence. The former is usually lower than the latter. M. Falcioni, G. Paladin and A. Vulpiani discussed the connection of this Lagrangian turbulence with behaviors of the velocity field [10] both in the Lorentz model [2] and in truncated Navier-Stokes equations. They indicate a possible road for the onset of Lagrangian turbulence which seems to be rather generic. It is found that the Lagrangian turbulence appears when the velocity field passes from a steady state to a periodic one via Hopf bifurcation. It is also shown that the transition to Eulerian turbulence does not affect the properties of particle motion as noted above. They further discussed an atypical example where it does not exhibit the Lagrangian turbulence even when it is chaotic in the Eulerian sense.

The transport properties of two-dimensional incompressible flow between adjacent convection rolls in the temporally oscillating Rayleigh-Bénard convection with a large aspect ratio were discussed by Solomon and Gollub both experimentally and theoretically [20]. The contents will be reviewed in § 3 in detail. The Rayleigh-Bénard convection is a hydrodynamic flow between horizontal layers heated from below. The fluid, in the incompressible case, is

governed by the hydrodynamic equations [5]

$$Pr^{-1}(\partial\vec{v}/\partial t + (\vec{v}\cdot\vec{\nabla})\vec{v}) = -\vec{\nabla}p + \vec{k}\theta + \vec{\nabla}^2\vec{v},$$

$$\partial\theta/\partial t + \vec{v}\cdot\vec{\nabla}\theta = R\vec{k}\cdot\vec{v} + \vec{\nabla}^2\theta,$$

$$\vec{\nabla}\cdot\vec{v} = 0, \tag{1.2}$$

with two nondimensional control parameters: the Rayleigh number R and the Prandtl number Pr. Here $\vec{v}$ denotes the velocity field, p the pressure, θ the temperature difference from the elemental temperature distribution, and $\vec{k}$ the unit vector in the vertical direction. Any flow type of the velocity field $\vec{v}$ is determined with a pair of the parameters, R, Pr, and the wave number α. When the Rayleigh number R increases, a time-independent laminar flow with $\alpha = 3.117$ appears at $R = R_c(= 1707)$. Busse et al. first studied how fundamental flow patterns can appear after the laminar flow becomes unstable [11], and some instabilities: oscillatory instability, skewed varicose instability, zig-zag instability, cross roll instability, etc., can be observed with the different Prandtl numbers and the wave numbers. The dependence of their instabilities on the Prandtl number Pr and the wave number α are exhibited in Fig. 1, which is referred to as the Busse balloon [11]. The oscillatory instability mainly appears in low Prandtl numbers, whereas, the zig-zag instability and the cross roll instability are important in high Prandtl numbers.

This property indicates that the Rayleigh-Bénard convection is a good model system for a comprehensive investigation of transport and diffusion,

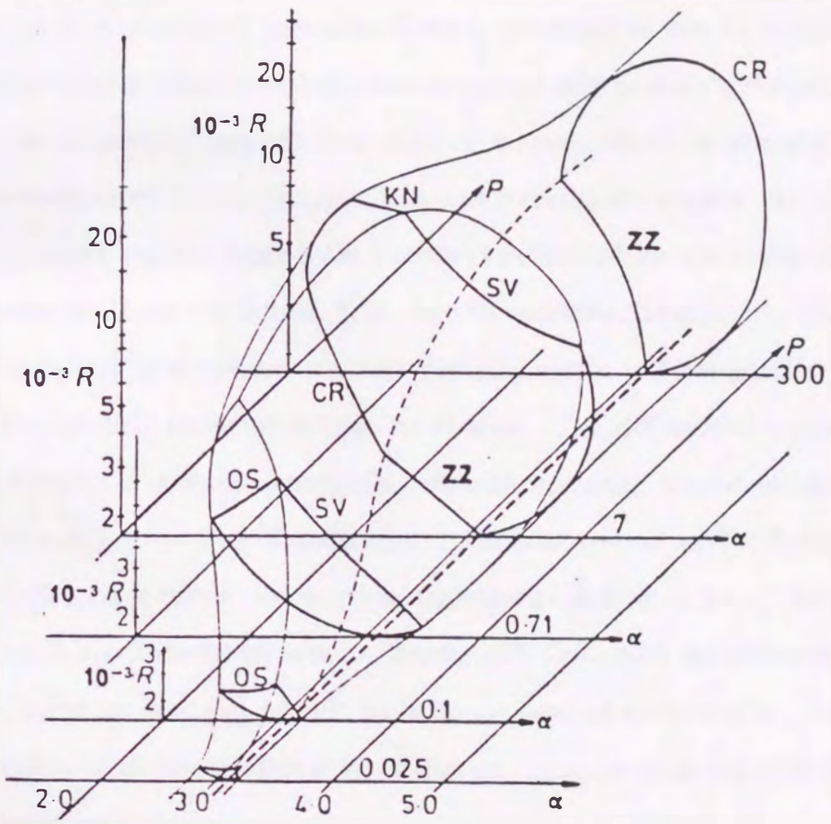

Figure 1: The dependence of the instabilities in the Rayleigh-Bénard convection; oscillatory instability, skewed varicose instability, zig-zag instability, cross roll instability, etc., on the Prandtl number Pr and the wave number α, which is obtained using the theoretical and experimental results [11]. (exhibited by F. H. Busse)

since convective flows can be created ranging from time-independent, spatially periodic flows on the one hand, to turbulent flows on the other. As a result, the transport rates vary over a wide range. At one extreme, when the fluid is motionless, the transport is due entirely to molecular diffusion. At the other extreme (turbulent flows), transport is due to advection by the flow and is often described phenomenologically as eddy diffusion. There are two important laminar flow regimes between these extremes in a low Prandtl number: a time-independent and a oscillating regime. In the time-independent regime, large-scale transport is limited by molecular diffusion between adjacent convection rolls. In the oscillating regime, the transport is dominated by advection of tracer particles across roll boundaries. In this regime, particle trajectories may be chaotic. The differential equation for the velocity of a fluid element in a two-dimensional, time-dependent flow are formally those of a Hamiltonian dynamical system with 1.5 degrees of freedom. As a result, the particle trajectories exhibit a lot of features of Hamiltonian chaos in real space. Chaotic structures such as heteroclinic tangles, invariant tori and islands have been observed numerically. Here, the quantitative effects of chaotic advection on transport and diffusion shall be discussed extensively.

In the present paper we shall especially show how the diffusion and mixing of passive particles by chaotic advection become anomalous when islands of tori exist [21, 22]. We shall use the stream function used by Solomon and Gollub to simulate the particle motion. They defined the diffusion constant

D in terms of Fick's law for the purpose of comparison with the experiment, measuring the value of D at most only for one complete period of oscillation. On the contrary, we shall adopt the statistical-mechanical definition of D which is determined by the asymptotic behavior of tracer particles over a long time. It is shown that the difference noted above causes important changes of the dependence of D on the amplitude B. In particular, there appear some fine-grained peaks in D vs B graph [21] which were not found by Solomon and Gollub. This peak structure is understood as the result of an enhanced transport of tracer particles which can be explained in terms of certain structures of the invariant manifolds in fluid space [21]. It is further shown as an extreme case of the enhanced transport that, in a peak range of B, there appear accelerator-mode islands on which particles move from $x = \mp\infty$ to $x = \pm\infty$ in the horizontal coordinate with a definite speed, so that the intermittent sticking to the islands leads to an anomalous diffusion with $D = \infty$ [22]. When they appear, the statistics of particle motions is dramatically changed and so physical quantities, too, as clarified recently for the standard map [25]. The formation mechanism of the accelerator-mode islands will be elucidated in terms of the lobe dynamics developed by Wiggins et al [26, 27].

As noted above, tracer particles diffuse in a widespread chaotic sea and this can be regarded as a stochastic process in a coarse-grained scale in spite that the dynamics is deterministic. This comes from an important feature of particle orbits in fluid space, i.e., the orbital instability due to the

exponential expansion of nearby particle orbits which leads to the mixing of tracer particles [20]. The existence of the mixing is indispensable for the presence of diffusion. The degree of mixing is quantified by the positive Liapunov exponent. The distribution function $P(\Lambda; n)$ of the coarse-grained expansion rates Λ_n gives us much more information on the particle orbits. In this thesis we shall also discuss the asymptotic form of $P(\Lambda; n)$ in the limit $n \to \infty$, and elucidate the anomalous mixing due to the coexisting normal islands. It should be noted here that, though each of the chaotic particle orbits is unstable against a small perturbation, their statistical properties over a sufficiently long time are stable and reproducible so that the statistical properties of particle orbits over a long time can be studied by computer simulation [23].

The present paper is organized as follows. In § 2 a review of dynamical systems is described. Here, the definitions of the Poincaré surface, unstable and stable manifolds, pips and lobs, etc., are given. The lobe dynamics noted here will play an important role of understanding the diffusion process from a deterministic point of view. In § 3 an experiment and a simulation by Solomon and Gollub are reviewed. In § 4 we describe the dependence of the diffusion constant D on the amplitude B of the roll oscillation of the velocity field, and discuss the fine-grained peaks. These results are compared with Solomon and Gollub's results, and the differences are elucidated. In § 5 we show the existence of accelerator-mode islands in a peak range of B and describe a few characteristics about them. In § 6 we treat the enhanced

diffusion and the accelerator-mode islands in terms of the lobe dynamics reviewed in § 2. In § 7 we discuss the spectrum $\psi(\Lambda)$ and the probability density $P(\Lambda; n)$ of the coarse-grained expansion rates Λ_n when islands exist. These quantities will show an anomalous scaling in this regime. A summary is given in § 8.

2 Review of Dynamical Systems

In this section, definitions and some properties for the equations of the following form are summarized:

$$dx/dt = f(x, t; \mu) \tag{2.1}$$

or

$$x \mapsto g(x; \mu) \tag{2.2}$$

where x is a D-dimensional vector, t means 'time' and μ are some parameters which control the properties of (2.1) or (2.2). We refer to (2.1) as a vector field or ordinary differential equation, and to (2.2) as a map or a difference equation. When (2.1) is solved with an initial condition x_0, a family of the orbits $x(x_0, t; \mu)$ or $\{x_0, x_1, x_2, \cdots\}$ is obtained, and the family is referred to as a dynamical system.

2.1 Poincaré map

The study of the continuous time systems (2.1) is reducible to the study of an associated discrete time system (2.2), by taking the Poincaré surface [1]. Nowadays virtually any discrete time system that is associated with an ordinary differential equation is referred to as a Poincaré map. This technique offers several advantages in the study of ordinary differential equations, including the following:

- Dimensional Reduction. Construction of the Poincaré map involves the elimination of at least one of the variables of the problem resulting in

the study of a lower dimensional problem.

- Global Dynamics. In lower dimensional problems (say, dimension ≤ 4) numerically computed Poincaré maps provide an insightful and striking display of the grobal dynamics of a system [29, 30].

- Conceptual clarity. Many concepts that are some what cumbersome to state for ordinary differential equations may often be simply stated for the associated Poincaré map.

An example would be the notion of orbital stability of a periodic orbit of an ordinary differential equation [12]. In terms of the Poincaré map, this problem would reduce to the problem of the stability of a fixed point of the map, which is simply characterized in terms of the eigenvalues of the map linearized about the fixed point as noted below.

The ordinary differential equation is easily reduced to a Poincaré map in the case where the phase space of the equation is periodic, such as in periodically forced oscillators. We consider the D-dimensional ordinary differential equation (2.1) and let $\phi(t, x; \mu)$ denote the solutions of (2.1), which form a one-parameter family of C^r, $r \geq 1$, diffeomorphism of the phase space. $\phi(t, x)$ is referred to as a phase flow or just a flow [13]. Let Σ be an $D-1$-dimensional surface transverse to the vector field at x_0 (note: "transverse" means that $f(x) \cdot n(x) \neq 0$ where "$\cdot$" denotes the vector dot product and $n(x)$ is the normal to Σ at x); we refer to Σ as a cross-section to the vector field (2.1). We can find an open set $V \subset \Sigma$ such that the trajectories starting

in V return to Σ in a time τ [13]. The map that associate points in V with their points of first return to Σ is called the Poincaré map, which is in terms of $\phi(t, \cdot; \mu)$ denoted as follows,

$$x \mapsto \phi(\tau(x), x; \mu) \tag{2.3}$$

where $\tau(x)$ is the time of first return of the point x to Σ. $\phi(\tau(x), x; \mu)$ is related with $f(t, x; \mu)$ as

$$\phi(\tau(x), x; \mu) = x + \int_0^{\tau(x)} f(t, x(t); \mu) dt. \tag{2.4}$$

Here after the properties of (2.2) is only stated because of the remark mentioned above.

2.2 Fixed points and their stability

Consider a general D-dimensional difference equation

$$x \mapsto g(x), \quad x \in R^D. \tag{2.5}$$

When a point x_0 is chosen, the orbit of x_0 under the map (2.5) is given by the infinite sequence $\{\cdots, f^{-n}(x_0), \cdots, f^{-1}(x_0), x_0, \cdots, f^n(x_0), \cdots\}$, and $f^n(x_0)$ is referred to as x_n. An fixed point of (2.5) is a point $\bar{x} \in R^D$ such that

$$\bar{x} = g(\bar{x}), \tag{2.6}$$

i.e., a solution which does not change in time. Then, roughly speaking, the fixed point $\bar{x}$ is stable if orbits $\{x_i\}$ starting "close" to $\bar{x}$ at a given time remain close to $\bar{x}$ for later times. It is asymptotically stable if nearby

solutions actually converge to $\bar{x}$ as $t \to \infty$. A fixed point is unstable if it is not stable. If $\bar{x}$ is an unstable fixed point, then there exists at least an orbit $\{x_n\}$ starting close to $\bar{x}$ at a given time and escaping from $\bar{x}$ for later times.

In order to determine the stability of $\bar{x}$, we must understand the nature of solutions near $\bar{x}$. Let $x = \bar{x} + y$, and substituting it into (2.5) and Taylor expanding about $\bar{x}$ gives

$$y' = Dg(\bar{x})y + \vartheta(|y|^2) \tag{2.7}$$

in terms of $\bar{x} = g(\bar{x})$, where Dg is the derivative of g and $|\cdot|$ denotes a norm on R^D. (2.7) from which higher order terms are removed describes the evolution of orbits near $\bar{x}$. $Dg(\bar{x})$ is, in this case, a matrix with constant entries, and the solution of (2.7) through the point y_0 of $n = 0$ can immediately be written as

$$y_n = e^{Dy(\bar{x})n} y_0. \tag{2.8}$$

Namely, if the eigenvalues of the associated linear map have not moduli one, then the orbit structure near on the fixed point of the nonlinear map is essentially determined by the eigenvalues [13].

Let $\bar{x}$ be a fixed point of (2.5). Then $\bar{x}$ is called a hyperbolic fixed point if none of the eigenvalues of $Dg(\bar{x})$ have Moduli one. A hyperbolic fixed point of the map is called a saddle if some, but not all, of the eigenvalues of the associated linearization have moduli greater than one and the rest of the eigenvalues have moduli less than one. If all of the eigenvalues have moduli less than one, then the hyperbolic fixed point is called a sink, and if all of the

eigenvalues have moduli greater than one, then the hyperbolic fixed point is called a source. If the eigenvalues have modulus one, the nonhyperbolic point is called a center. It should be clear that the fixed point $y = 0$ of the linear map (2.7) is asymptotically stable if all the eigenvalues of $Dg(\bar{x})$ have moduli strictly less than one, which means that $\bar{x}$ is a sink. On the other hand, if $\bar{x}$ is source or saddle, then the fixed point is unstable.

2.3 Invariant manifolds

We will see that invariant manifolds, in particular stable and unstable manifolds, play an important role in the analysis of the structures of dynamical systems. We will restrict a discussion of these ideas only to a map (2.5). Let $S \subset R^D$ be a set. S is said to be invariant under the map $x \mapsto g(x)$ if for any $x_0 \in S$ we have $g^n(x_0) \in S$ for all n. We remark that if g is noninvertible, then only $n \geq 0$ makes sense, although in some instances it may be useful to consider g^{-1}. An invariant set $S \subset R^n$ is said to be an invariant manifold if S has the structure of a differentiable manifold. Roughly speaking, a manifold is a set which locally has the structure of Euclidean space [14].

The stable and unstable manifold of a fixed point $\bar{x}$, $W^{\mathrm{s}}(\bar{x})$, $W^{\mathrm{u}}(\bar{x})$ are defined by [30]

$$W^{\mathrm{s}}(\bar{x}) = \{x \in R^D | g^n(x) \to \bar{x} \text{ as } n \to +\infty\},$$

$$W^{\mathrm{u}}(\bar{x}) = \{x \in R^D | g^{-n}(x) \to \bar{x} \text{ as } n \to -\infty\}, \tag{2.9}$$

respectively. It is easily shown in terms of the above definition that the set $W^{\mathrm{s}}(\bar{x})$ is invariant under the map $x \mapsto g(x)$. For any $x \in W^{\mathrm{s}}(\bar{x})$, $g^n \circ g(x) =$

$g^{n+1}(x) \to \bar{x}$ as $n \to +\infty$, and so $g(x)$ is also an element of $W^s(\bar{x})$, or equally $g(W^s(\bar{x}))$ is a subset of $W^s(\bar{x})$. We can also show that $W^s(\bar{x})$ is a subset of $g(W^s(\bar{x}))$ with the similar way. The two relations: $g(W^s(\bar{x})) \subset W^s(\bar{x})$ and $W^s(\bar{x}) \supset g(W^s(\bar{x}))$, say that $W^s(\bar{x}) = g(W^s(\bar{x}))$. By repeating the above process, the relation is easily generalized to $W^s(\bar{x}) = g^n(W^s(\bar{x}))$ for any n, and hence $W^s(\bar{x})$ is an invariant set.

Two stable (or unstable) manifolds, $W^s(\bar{x}_1)$ and $W^s(\bar{x}_2)$ of distinct fixed points $\bar{x}_1$, $\bar{x}_2$ cannot intersect each other. If $W^s(\bar{x}_1)$ and $W^s(\bar{x}_2)$ intersect at a point x, then $g^n(x) \to \bar{x}_1$ in the limit $n \to \infty$ since x is an element of $W^s(\bar{x}_1)$, at the same time, $g^n(x) \to \bar{x}_2$ in the limit $n \to \infty$ since x is also an element of $W^s(\bar{x}_2)$. As a result, existence and uniqueness of solutions of $(2 \cdot 5)$ ensure that $W^s(\bar{x}_1) \cap W^s(\bar{x}_2) = \emptyset$. On the other hand, intersections of stable and unstable manifolds of distinct fixed points can occur, and indeed, are a source of the complex structure of phase space found in dynamical systems. If there exists an intersection x of stable and unstable manifold $W^s(\bar{x}_1)$, $W^u(\bar{x}_2)$, then there also exist infinite intersections $\{g^n(x)\}$ for all n, since $W^s(\bar{x}_1)$ and $W^u(\bar{x}_2)$ are invariant under the map g.

We then illustrate a separatrix as a simple example of $W^s(\bar{x})$ and $W^u(\bar{x})$. We limit, for simplicity, a system with one-degree of freedom i.e., a vector field on a two-dimensional phase space, that have a first integral that can be viewed as the sum of a kinetic and potential energy. As a preliminary step, the shape of the potential $V(x)$ is assumed to be a double-well potential where a coordinate $(x, y) = (0, 0)$ is the maximum. Now suppose that the

first integral is given by

$$h = y^2/2 + V(x),$$

and then

$$y = \pm\sqrt{2}\sqrt{h - V(x)}. \tag{2.10}$$

Our goal is to draw an orbit with $h = 0$. Imagine sitting at the point $(0,0)$, with h fixed. Now move toward the right, i.e., let x increase. Then, since $y = +\sqrt{2}\sqrt{h - V(x)}$ and h is fixed, y must increase until the minimum of the potential is reached, and then it decreases until the boundary of the potential is reached. In the case that h is equal to the maximum value, all the points $\{x(t), y(t)\}$ reach a fixed point $\{0,0\}$ in the limit $t \to -\infty$; hence the set $\{x, \sqrt{2}\sqrt{-V(x)}\}$ is an unstable manifold $W^{\mathrm{u}}(0,0)$. Now $y = +\sqrt{2}\sqrt{h - V(x)}$ to $-\sqrt{2}\sqrt{h - V(x)}$ as time increases, and in the case of $h = 0$, the points $\{x(t), y(t)\}$ also reach the fixed point $\{0,0\}$ in the limit $t \to \infty$; hence the set $\{x, \sqrt{2}\sqrt{-V(x)}\}$ is also a stable manifold $W^{\mathrm{s}}(0,0)$. Since $W^{\mathrm{u}}(0,0)$ is accordance with $W^{\mathrm{s}}(0,0)$ in this case, $W^{\mathrm{u}}(0,0)(= W^{\mathrm{s}}(0,0))$ forms a loop including the fixed point $\{0,0\}$. All the points on the loop reach $\{0,0\}$ in both the limit $t \to \pm\infty$, and the orbit is sometimes called a separatrix, since it is a boundary between two distinctly different types of motions. Namely, if h is grater than the maximum value 0 of the potential energy $V(x)$, then the particle go around the right- and the left-well. For $h < 0$, within the potential well, the value of initial energy corresponds to bounded motion. The separatrices and the generalized ones will play an important role of analyzing the transport and the diffusion of tracer particles.

2.4 Pips and lobes

Consider a two-dimensional map g with a control parameter μ

$$g : R^2 \mapsto R^2 \tag{2.11}$$

with a hyperbolic periodic point p_0, i.e., for some integer $k \geq 1$, $g^k(p_0) = p_0$. Without loss of generality we can assume that $k = 1$ by applying our argument to g^k rather than g. As an additional technical assumption we suppose that g is orientation preserving, i.e., $\det Dg > 0$. If g does not preserve orientation, then we apply our argument to g^2, which does preserve orientation. It is natural since Poincaré maps arising from vector fields preserve orientation. We assume that an separatrix exists on some value of μ. When μ is changed, the separatrix often separates into an unstable and a stable manifold of the fixed point p_0, $W^{\mathrm{u}}(p_0)$ and $W^{\mathrm{s}}(p_0)$, respectively, and the manifolds often intersect transversely. We denote one of the intersection points as q, and the point is said to be homoclinic to p_0 or simply a homoclinic point. If $W^{\mathrm{s}}(p_0)$ and $W^{\mathrm{u}}(p_0)$ are transversal at q, then q is called a transversal homoclinic point. Consider an orbit of q under g

$$\{\cdots, g^{-2}(q), g^{-1}(q), q, g(q), g^2(q), \cdots\}. \tag{2.12}$$

Since q lies in both $W^{\mathrm{s}}(p_0)$ and $W^{\mathrm{u}}(p_0)$, and these manifolds are invariant, the infinite number of points in (2.12) must lie in both $W^{\mathrm{s}}(p_0)$ and $W^{\mathrm{u}}(p_0)$. Therefore, $W^{\mathrm{s}}(p_0)$ and $W^{\mathrm{u}}(p_0)$ must wind amongst each other intersecting along the infinite number of points given in (2.12). This geometrical structure

has been called a homoclinic tangle, and we now develop the concepts to describe it more quantitatively.

Let $U[g^{-1}(q), q]$ denotes the segment of $W^{u}(p_0)$ with end points at $g^{-1}(q)$ and q. Then $W^{s}(p_0)$ intersects $U[g^{-1}(q), q]$ at q and $g^{-1}(q)$ and also at k points in between q and $g^{-1}(q)$ with $k \geq 1$ for orientation preserving maps. Without loss of generality we can assume $k = 1$, and easily generalize our results for $k > 1$. We denote the segment of $W^{s}(p_0)$ with endpoints at q and $g^{-1}(q)$ by $S[g^{-1}(q), q]$. Here we call a special type of homoclinic point q as a primary intersection point or pip defined as follows. Suppose $q \in W^{s}(p_0) \cap W^{u}(p_0)$. Then q is called a primary intersection point(pip) [15] if, other than p_0, $S[p_0, q]$ and $U[p_0, q]$ intersect only in the point q. The following lemma [26], which is easily proved, is quite useful.

Lemma. *If q is a pip, then $g^{k}(q)$ is a pip for any k.*

Lemma determines how to iterate of $U[g^{-1}(q), q]$ and $S[g^{-1}(q), q]$ with g, and of a lobe L, which is defined as follows. Let q and q_1 be two adjacent pips i.e., there are no other pips on $U[q, q_1]$ (or equivalently $S[q, q_1]$) between q and q_1. Then we refer to the region bounded by $U[q, q_1]$ and $S[q, q_1]$ as a lobe. For any lobe L, $\mu(L)$ will denote the area of L. From lemma and the invariance of $W^{s}(p_0)$ and $W^{u}(p_0)$, it follows that, for any lobe L, $g^{k}(L)$ is also a lobe for any k. However, besides the pips, there are other secondary intersection points or sips which complicate matters further. Consider the lobes labeled L_1 and L_2 in Fig. 2. Then, for positive integers k and n sufficiently large, $g^{k}(L_1)$ must cut through $g^{-n}(L_2)$ as shown in Fig. 2.

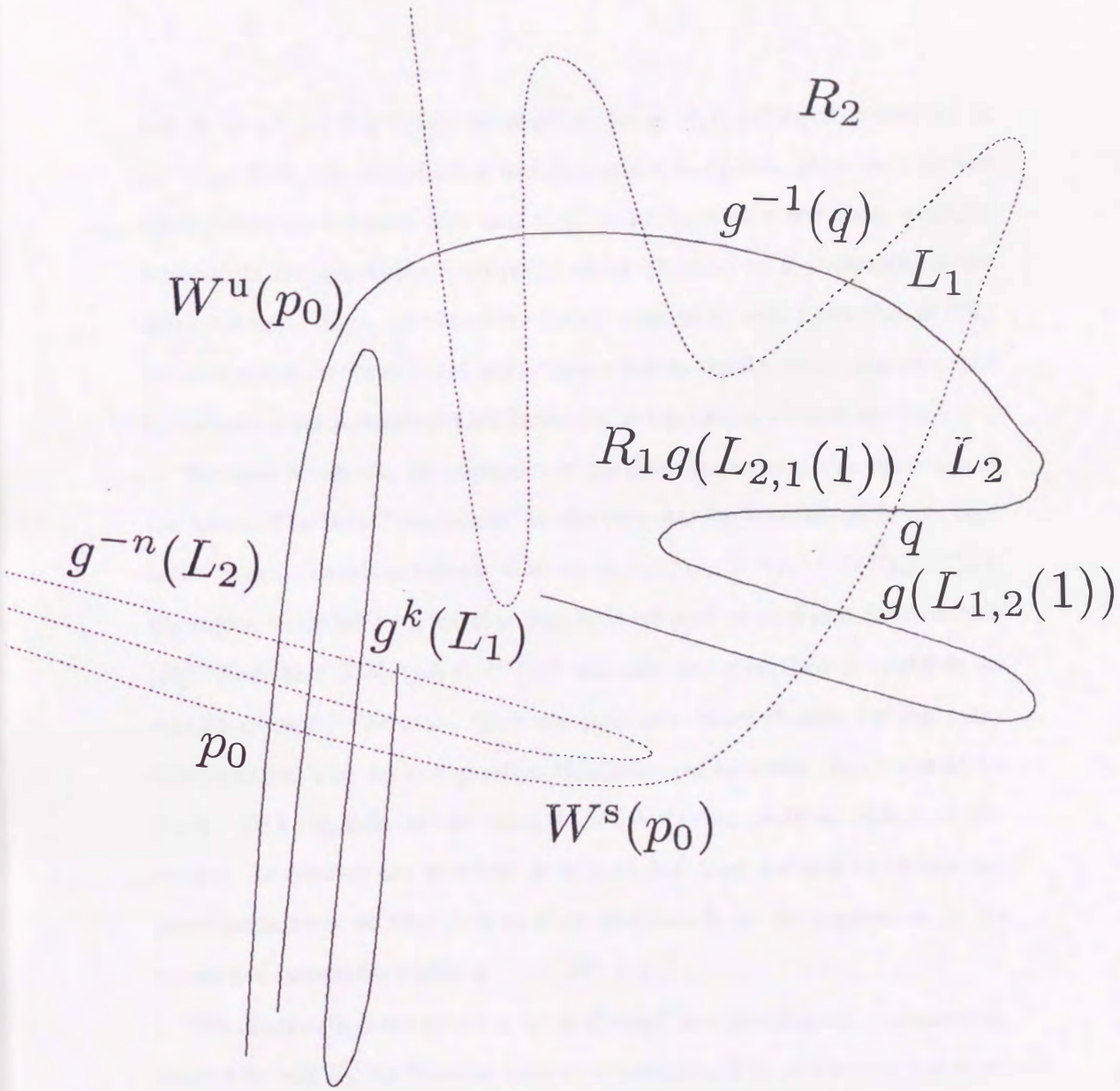

Figure 2: Stable and unstable manifold, $W^{\mathrm{s}}(p_0)$, $W^{\mathrm{u}}(p_0)$ are shown with lobes L_1, L_2, $g(L_{1,2}(1))$, $g(L_{2,1}(1))$.

Let $X = g^k(L_1) \cap g^{-n}(L_2)$; then $g^n(X) = g^{n+k}(L_1) \cap L_2$ is contained in L_2. Therefore, iterates of lobes will intersect other lobes. Here we note the main difference between pips and sips. Namely, once a pip enter a neighborhood of the hyperbolic fixed point under iteration by g, it remains in the neighborhood. Sips, on the other hand, may enter and leave the vicinity of the hyperbolic fixed point many times before finally remaining near the hyperbolic fixed point under all forward (or backward) iterations by g.

We then formulate the transport of particles in terms of the dynamics of the lobes. The term "separatrix" in the map having transversal homoclinic orbits is generalized as follows. Choose any pip $q \in W^s(p_0) \cap W^u(p_0)$. Then the region bounded by $U[p_0, q] \cup S[p_0, q]$ is referred to as a pseudoseparatrix [26]. Note that if $W^s(p_0) \cap W^u(p_0)$ contains one pip, then it contains an infinity of pips. Therefore, there are infinitely many choices for the pseudoseparatrix. The obvious question thus arises as to which choice should be made. This depends on the context of the specific problem under consideration. In dealing our problem, it is probably most natural to choose the pseudoseparatrix so that it is as close as possible to the separatrix in the associated integrable problem.

We assume that the phase space is divided into two disjoint components, labeled R_1 and R_2, by choosing a pseudoseparatrix. The problem of transport in phase space that we shall study is concerned with how initial points in R_1 may enter R_2. It will be shown that this is completely determined by the geometry and dynamics of the lobes. We suppose that $S[g^{-1}(q), q]$ intersects

$U[g^{-1}(q), q]$ in precisely one pip besides $g^{-1}(q)$ and q, as shown in Fig. 2. Then precisely two lobes are formed, one lying in R_1 and the other lying in R_2, which we denote by $L_{1,2}(1)$ and $L_{2,1}(1)$, respectively. Now $g(L_{1,2}(1))$ and $g(L_{2,1}(1))$ appear as in Fig. 2. Note that $L_{1,2}(1)$ enters R_2 under one iteration by g, and $L_{2,1}(1)$ enters R_1 under one iteration by g. This is the mechanism for transport across the pseudoseparatrix and appears to have been discussed explicitly for the first time by Channon, Lebowitz [16] and Bartlett [17]. The lobes bounded by $U[g^{-1}(q), q] \cup S[g^{-1}(q), q]$ have been called a turnstile by Mackay, Meiss and Percival [35]. The mechanism for transport noted above reveals that initial points in R_i entering R_j on the n-th iterate of g must be in $L_{i,j}(1)$ on the $(n-1)$ iteration of g, with $i, j = 1, 2$.

Now we can obtain an important quantity concerning the transport in phase space across the pseudoseparatrix. The area of phase space crossing the pseudoseparatrix from R_1 into R_2 under one iteration of g is given by $\mu(g(L_{1,2}))$. Thus, the total area of phase space crossing the pseudoseparatrix from R_1 into R_2 under n iterations of g is $n\mu(g(L_{1,2}))$. The quantity we want to obtain is the area occupied by points that are in R_1 initially (i.e., at $t = 0$) that enter R_2 on the n-th iteration by g. The quantity is not $\mu(g(L_{1,2}))$, because we are not just interested in arbitrary points crossing the pseudoseparatrix but, rather, in points which have a specified location initially. Thus, with each point in the plane it is important to keep track of whether it was in R_1 or R_2 initially. The points lying in R_i at $t = 0$ will be called R_i particles. Heuristically, we can think of R_1 particles as black fluid

and R_2 particles as white fluid, and we are interested in how the fluid mix amongst each other under the dynamics generated by g. We first establish some definitions. Let $L_{i,j}(n)$ denote the lobe that leaves R_i and enters R_j on the n-th iterate and let

$$L^k_{i,j}(n) \equiv L_{i,j}(n) \cap R_k; \tag{2.13}$$

thus we have

$$g^{n-1}(L_{i,j}(n)) \equiv L_{i,j}(1). \tag{2.14}$$

The main quantity that we wish to compute is a flux of R_i particles into R_j on the n-th iterate, which is given from these definitions by

$$\mu(g^n(L^1_{1,2}(n))). \tag{2.15}$$

Next we want to compute $L^1_{1,2}(k)$. Using an observation noted above, R_1 particles can not enter R_2 on the k-th iterate unless it is in $L_{1,2}(1)$ on the $(k-1)$ iterate. Thus, points in $g^{-k+1}(L_{1,2}(1))$ enter R_2 on the k-th iterate. However, $g^{-k+1}(L_{1,2}(1))$ may not contain only R_1 particles, since $g^{-k+1}(L_{1,2}(1))$ may intersect $g^{-l+1}(L_{2,1}(1))$, $l = 1, \cdots, k$, and, thus, lie in R_2. Hence we have

$$L^1_{1.2}(k) = g^{-k+1}(L_{1,2}(1)) - \bigcup_{l=0}^{k-1}(g^{-k+1}(L_{1,2}(1)) \cap g^{-l}(L_{2,1}(1))).$$

Now, since the sets $g^{-k+1}(L_{1,2}(1)) \cap g^{-l}(L_{2,1}(1))$ are disjoint, we have

$$\mu(g^n(L^1_{1,2}(k))) = \mu(g^{n-k+1}(L_{1,2}(1))) - \sum_{l=0}^{k-1}\mu(g^{n-k+1}(L_{1,2}(1)) \cap g^{n-l}(L_{2,1}(1))).$$

Thus the flux $\mu(g^n(L^1_{1,2}(n)))$ is obtained as [26]

$$\mu(g^n(L^1_{1,2}(n))) = \mu(g(L_{1,2})) - \sum_{k=0}^{n-1}\mu(g(L_{1,2}(1)) \cap g^{n-k}(L_{2,1}(1)))). \tag{2.16}$$

We make an important remark that (2.16) has implications for all points in R_1 but are obtained entirely by iterating the turnstile. The formula will be used in § 6 and play an important role of elucidating the diffusion process of the Rayleigh-Bénard convection from a deterministic point of view.

2.5 Dissipative and conservative systems

The D-dimensional differentional equations $dx/dt = f(x)$ are called dissipative systems when the phase space volume is continuously contracted with increasing time, and then the contraction rate is given by $\nabla \cdot f < 0$. This leads to contraction onto a surface of lower dimensionality than the original phase space, and the surface is referred to as the attractor. For regular motion, the attractor of the flow represents a simple motion such as a fixed point (sink) or a singly periodic orbit (limit cycle). For flows in two-dimensions there are , in fact, the only possibilities.

For three-dimensional regular flows, in addition to sinks and limit cycles, quesiperiodic orbits may be possible. In addition to these simple attractors, it has been shown that attractors exist for dissipative flows in three- or more-dimensions that have very complicated geometric structures. These structures can be characterized as having a fractional dimension, and are usually called strange attractors. The motion on strange attractors is chaotic or critical.

On the other hand, the differentional equations are called conservative systems or Hamiltonian systems when the phase space volume is conserved,

which satisfy the condition $\nabla \cdot f(x) = 0$, or $\det Dg = 1$ in the case of a map g. If a $2n$-dimensional equation is determined by a Hamiltonian function $H(q,p,t)$ as

$$\begin{aligned} dp_i/dt &= -\partial H/\partial q_i \\ dq_i/dt &= \partial H/\partial p_i, \quad i = 1, \cdots, n, \end{aligned} \tag{2.17}$$

then the equations always satisfy the conservative condition as follows,

$$\nabla \cdot f(x) = \sum_{i=1}^{n} \frac{\partial}{\partial p_i}(-\frac{\partial H}{\partial q_i}) + \frac{\partial}{\partial q_i}(\frac{\partial H}{\partial p_i}) \equiv 0.$$

Consider a time-independent Hamiltonian system $H_0(q,p)$ with n-degrees of freedom. If there exist n-independent invariants of the motion, then the system is called integrable. It is well known as the Arnold theorem that the flow of the integrable system with n-degrees of freedom forms n-dimensional tori. We then consider a $2n$-dimensional integrable system that is perturbed slightly. If the perturbation is sufficiently small, the KAM theorem [18] guarantees the existence of invariant tori. The theorem says that if the linear independence condition of the frequencies is satisfied with over some domain of phase space, then the perturbed motion is much less than the unperturbed one and the invariant curves, which is called KAM-invariant curves, exist near the unperturbed orbits. In the region that the condition is not satisfied, chains of alternating elliptic and hyperbolic fixed points are found with regular phase space trajectories encircling the elliptic fixed points and invariant manifolds connecting to the hyperbolic points. The stochastic behavior of the map around the hyperbolic points is found and is understood

due to the sequential stretching- and folding processes in phase space, and the processes are visualized with the homoclinic (or heteroclinic) tangles of the invariant manifolds.

The transport property of particles are, as noted above, analyzed in terms of the lobe dynamics. The Hamiltonian system has neither sinks nor sources, and hence the lobe dynamics will be more simple [26]. We again limit to the map g with $\det Dg = 1$. In this case we have

$$\mu(g(L_{1,2}(1))) = \mu(L_{1,2}(1)), \tag{2.18}$$

and

$$\mu(g(L_{1,2}(1)) \cap g^{n-k}(L_{2,1}(1))) = \mu(L_{1,2}(1) \cap g^{n-k-1}(L_{2,1}(1))). \tag{2.19}$$

Substituting (2.18) and (2.19) into (2.17), and reindexing gives

$$\begin{aligned} \mu(g^n(L^1_{1,2}(n))) &= \mu(L^1_{1,2}(n)) \\ &= \mu(L_{1,2}(1)) - \sum_{k=1}^{n-1} \mu(L_{1,2}(1) \cap g^k(L_{2,1}(1))), \end{aligned} \tag{2.20}$$

where we have used the fact that by construction $L_{1,2}(1) \cap L_{2,1}(1) = \emptyset$. In words, the sets $L_{1,2}(1) \cap g^k(L_{2,1}(1))$ are the points that leaves R_1 and enter R_2 under one iteration by g subject to the condition that they entered R_1 from R_2 k iterations earlier.

3 An Experiment on Diffusion by Solomon and Gollub

Solomon and Gollub have studied the transport of tracer particles in nearly two-dimensional, time-periodic Rayleigh-Bénard convection experimentally and numerically [20]. In their paper qualitative observations of the transport rates are presented, along with quantitative measurements of the transport rates as a function of the strength of the time dependence. A simplified numerical model is discussed in which transport between convection rolls is caused by chaotic advection due to lateral oscillations of the roll boundaries. Then the model gives a semiquantitative account of the experimental results.

3.1 Diffusion of tracer particles in Rayleigh-Bénard convection

The convection cell used in their experiments is a rectangular box with horizontal dimensions $15cm$ (along the x direction) by $1.5cm$ (the y direction) and a depth of $0.75cm$ (z direction). The working fluid is water at an average temperature of $36\,^{\circ}C$, where the Prandtl number is 4.7. Convection patterns are established with rolls oriented parallel to the short side of the convection cell. To obtain spatial information about the flow it is necessary to collect velocity time series at locations along the convection cell. The time average value of the vertical velocity $\bar{v}_z$ at each location is then used to describe the spatial structure of the flow, and the standard deviation $< \sigma_v >$ averaged over a wave-length of the flow is used as a measure of the local

amplitude of time dependence. After injection of an impurity, which is referred to as tracer particles elsewhere, one-dimensional concentration profiles $c(x,t)$ averaged over y and z direction are measured at the midhight of the cell. An enhanced local-transport coefficient is defined using Fick's law for a coarse-grained concentration profile $c(x,t)$:

$$F(x,t) = D(x,t)\frac{\partial c(x,t)}{\partial x}, \tag{3.1}$$

where $F(x,t)$ is the flux of dye past the point x at t and $\partial c/\partial x$ is determined by measuring the slope of $c(x,t)$ between the centers of adjacent convection rolls. The enhanced diffusion coefficient $D(x,t)$ is determined by dividing $F(x,t)$ by $\partial c/\partial x$.

Transport experiments were performed at Rayleigh number R ranging from $R/R_c = 19$ (just above the onset of time dependence in this cell) through $R/R_c = 32$. Here R_c is the Rayleigh number corresponding to the onset of convection. Visual observation of the motion of an impurity injected through a small tube in the bottom corner of the cell clearly indicates the presence of advective transport between convection rolls. Small blobs of the impurity are pulled periodically from the corner of one roll into the next. Lines of impurity are stretched and folded repeatedly in the vicinity of the corners. Stretching and folding of this nature are common characteristics of chaotic maps in which a rectangle in phase space is stretched and folded onto itself. Within the rolls, impurity concentrations are found to homogenize very rapidly. This time is short compared to the typical time of approximately one-half day for the experiments.

Transport coefficients are measured for each run in terms of (3.1), which is found to be independent of time, within the resolution of the data. There is a monotonic relationship between D and $< \sigma_v >$ which we determined experimentally. Plots of D vs $< \sigma_v >$ are shown in Fig. 3 with open circles. An approximately linear relationship can be seen from these plots.

3.2 Elucidation in terms of Lagrangian turbulence

A simplified model of transport in time-periodic Rayleigh-Bénard convection is, then, described. A Lagrangian approach is taken in which the trajectories of individual tracer particles are obtained by integrating the equations describing the velocity field. The system is Hamiltonian: $dx(x,z,t)/dt$ and $dz(x,z,t)/dt$ are derived from a stream function

$$\Psi(x,z,t) = (A/k)\sin\{k[x + B\sin(\omega t)]\}W(z), \tag{3.2}$$

where A is the maximum vertical velocity in the flow, k is the wave number $2\pi/\lambda$, and $W(z)$ is an even function of z that satisfies the rigid boundary condition at the top and bottom surfaces. $W(z)$ is obtained by solving the hydrodynamic equations (1.2) strictly [28]. This stream function describes single-mode two-dimensional convection with rigid boundary conditions. $B = 0$ corresponds to the flow where the Rayleigh number R is below the onset of the time-dependent instability. To study the flow above the onset, the term $B\sin(\omega t)$ is inserted, and the term represents the lateral oscillation of the roll pattern with amplitude B and frequency ω that is caused by the even oscillatory instability [19].

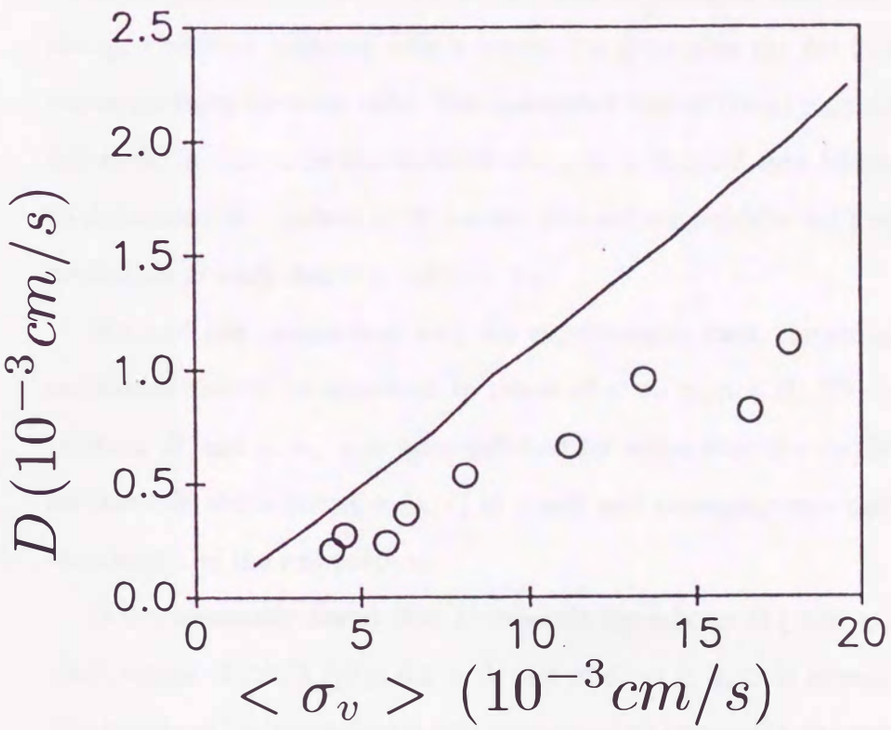

Figure 3: Quantitative comparison between simulation (solid line) and experiment (open circle) for the diffusion constant.

Trajectories of particles near the separatrices are chaotic in this model. A quantitative comparison can be made between the model and the experimental transport data. Calculations of D as a function of B have been performed for the model. The parameters A and ω are set to match the conditions of the experiment. One convection roll is filled uniformly with 10000 particles, and the trajectories of these particles are computed individually. After one complete period of oscillation, the number of particles that have been exchanged between adjacent rolls is counted to determine the net flux $F(x,t)$of tracer particles between rolls. The calculated flux of tracer particles and the difference in concentration between the rolls is inserted into Fick's law (3.1) to determine D. Values of D are determined numerically for amplitude of oscillation B such that $0 < 2B/\lambda < 0.1$.

For a proper comparison with the experimental data, the strength of the oscillation should be expressed in terms of $< \sigma_v >$, not B. The convection between B and $< \sigma_v >$ is accomplished by expanding the $\partial z/\partial t$ equation for small B, determining $\sigma_v(x,z)$ at $z = 0$ and averaging over one complete wavelength of the roll pattern.

It is numerically found that D depends linearly on B (and $< \sigma_v >$) for small values of $2B/\lambda$ ($0 \leq 0.1$). A plot of D vs $< \sigma_v >$ is shown in Fig. 3. The results of the numerical model are presented along with the experimental data. For both the experimental and numerical data, D scales linearly with $< \sigma_v >$. The slopes of the experimental and numerical data differ by about a factor of 2.

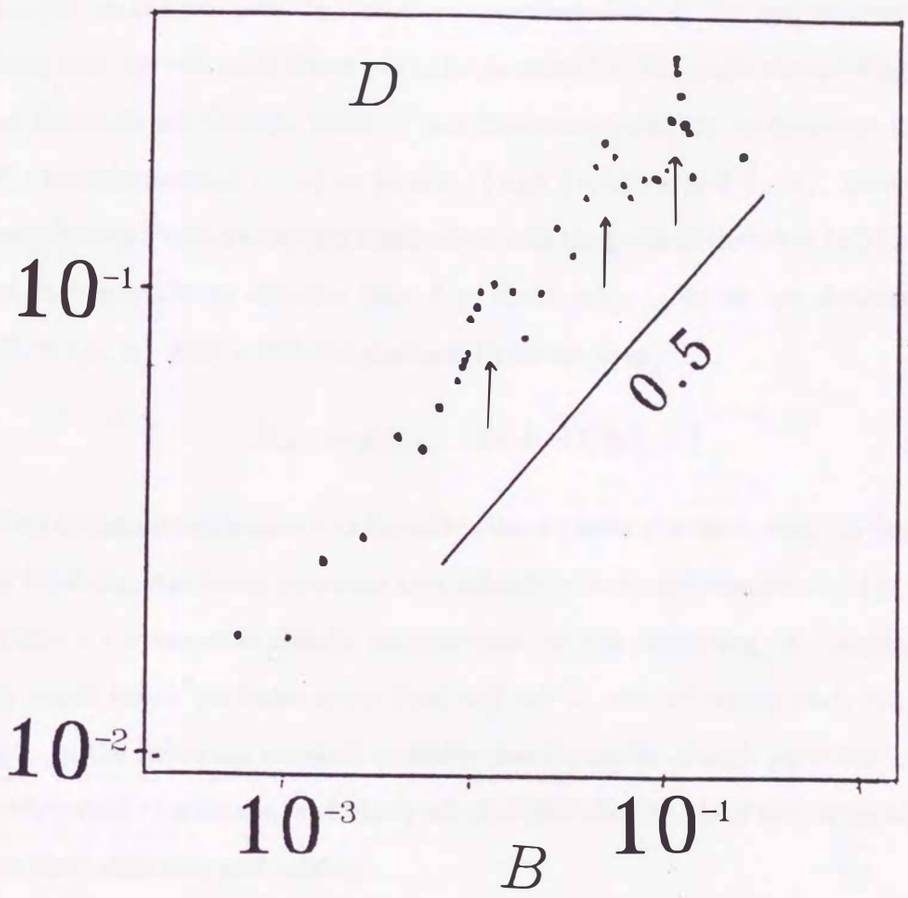

Figure 4: Diffusion constant D vs amplitude B ($= 10^{-3} \sim 10^{-1}$) of lateral oscillation, which is obtained from (4.2) with both the ensemble average over 100 tracer particles distributed on the line $x = 0$ uniformly at $t = 0$ and the time average with respect to each tracer particle over $t = 0 \sim 5000$. The vertical arrows indicate the three peaks at $B = 0.012$, 0.097 and 0.16.

4 Some Characteristics of Diffusion Constant

The diffusion constant D measured by Solomon and Gollub is reflected only in properties of a few periods of motion, as reviewed in § 3. We now examine the long-time behaviors of tracer particles governed by the same stream function as Solomon and Gollub, which is nondimensionarized, to be invariant under the transformations $\{x, z\} \to \{x \pm 2, z\}$ and $\{x, z\} \to \{x \pm 1, -z\}$. Using the well-known Poincaré-section method we take the plots of the orbit $\{x(t), z(t)\}$ of each particle at discrete time $t = 0, \pm 1, \pm 2, \cdots$, which are denoted by $X_t \equiv \{x_t, z_t\}$ with a two-dimensional Poincaré map

$$X_{t+1} = g(X_t). \quad (t = 0, \pm 1, \pm 2, \cdots) \tag{4.1}$$

This system is equivalent to a Hamiltonian dynamical system with 1.5 degrees of freedom, exhibiting invariant tori, islands of tori, and chaotic seas [29, 30]. There is a widespread chaotic sea generated by the oscillating roll boundaries, in which tracer particles move from roll cell to roll cell successively [20, 21, 22]. In the following we shall consider chaotic orbits of such particles in the widespread chaotic sea, and study what effects the islands of tori bring about on their diffusion and mixing.

The motion of each particle in this chaotic sea is characterized as a diffusion process in the horizontal direction because the memory of its initial point is lost rapidly due to the mixing of particle orbits, and can be regarded

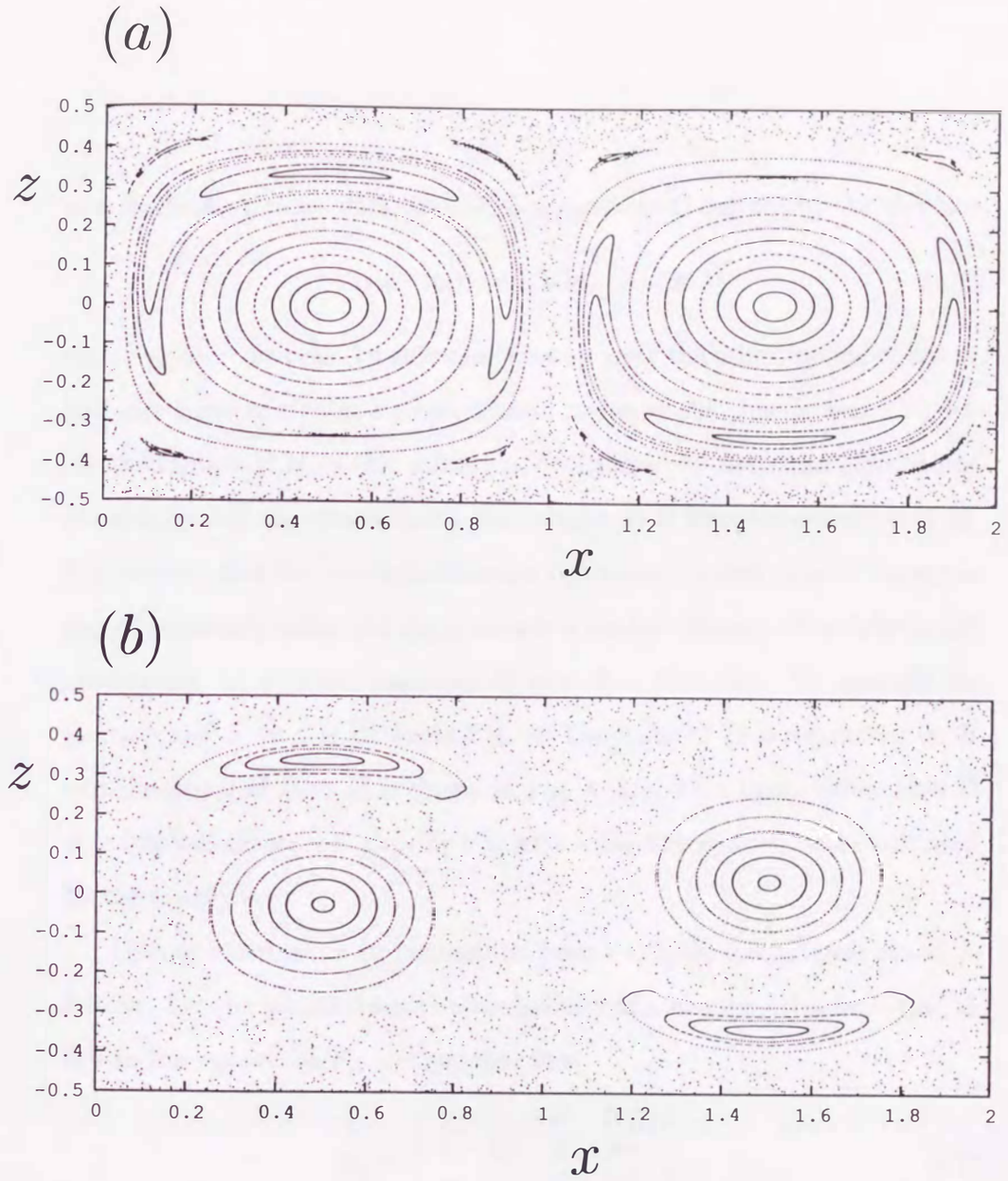

Figure 5: A widespread chaotic sea and two islands for (a) $B = 0.01$ and (b) $B = 0.05$. Scattered dots represent the chaotic sea. Each island consists of a complicated mixture of invariant tori and bounded chaotic regions, and is encircled by a critical torus.

as a stochastic process with the diffusion constant D defined by the variance

$$< (x_n - x_0)^2 >= 2Dn, \quad (n \gg 1) \tag{4.2}$$

where $< \cdots >$ denotes the ensemble average over the initial points of tracer particles concentrated in a small chaotic region of the chaotic sea. The diffusion constant D is, in this definition, determined by long-time correlations of particles, and shows a different dependence on B from the definition (3.1). It is obvious that the two definitions are equivalent to each other if the equation of continuity holds and the system is a markov process. D is determined numerically for different values of B with $0 < B < 0.2$. An example for $< (x_n - x_0)^2 >$ vs n is shown in Fig. 6. The value of D is dependent on B and the graph of D vs B is shown in Fig. 4 [21]. This figure shows that D depends linearly on $\sqrt{B}$ globally but with some fine-grained peaks indicated by the arrows.

The dependence can be understood from a simplified stochastic model as follows. Let the lateral transition probability of a chaotic orbit from the ith cell to the jth cell be P_{ji} and suppose that

$$P_{ji} = \begin{cases} p & \text{if} \quad \text{j=i+1}, \\ 1-2p & \text{if} \quad \text{j=i}, \\ p & \text{if} \quad \text{j=i}-1, \\ 0 & \text{otherwise}, \end{cases} \tag{4.3}$$

where $\sum_j P_{ji} = 1$. Then (4.2) with $n = 1$ leads to $D = (1/2)\sum_j (j-i)^2 P_{ji} = p$. Let C_i be the widespread chaotic region of the ith cell R_i whose particles can be transported into its neighboring cells $R_{i\pm1}$, and $\mu(C_i)$ be its area. The accelerator-mode islands will be included in C_i, in existing the islands. The

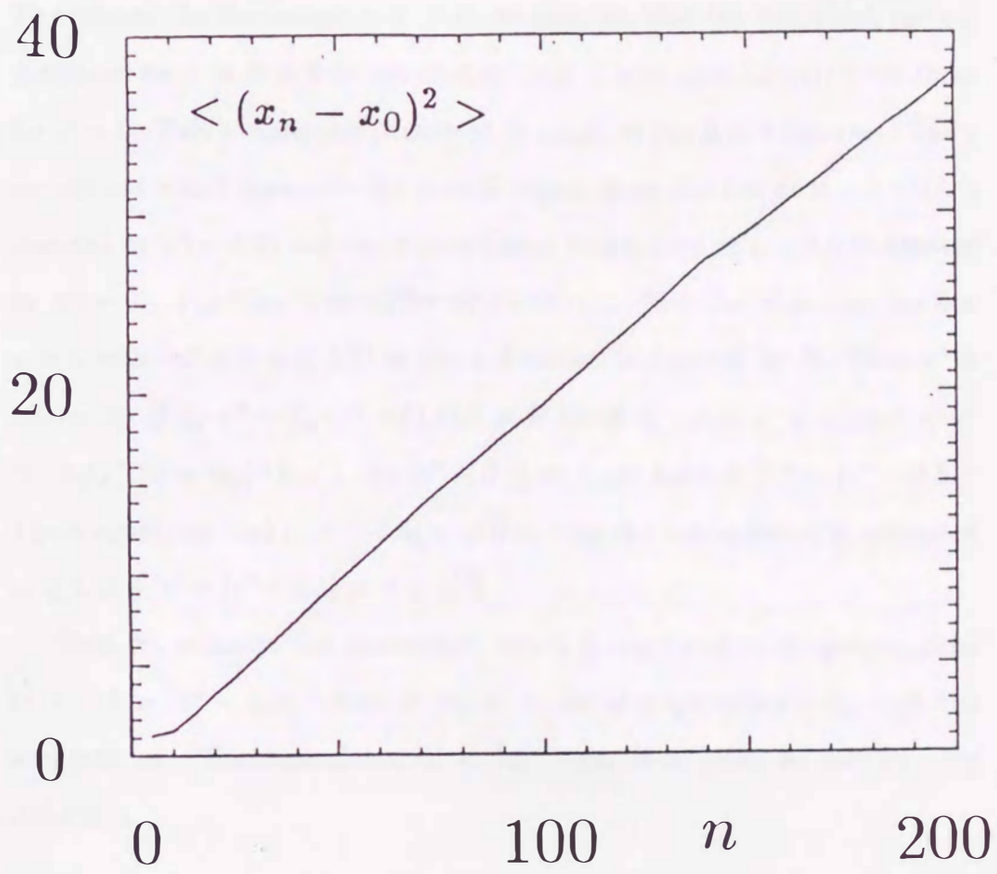

Figure 6: $< (x_n - x_0)^2 >$ vs n for $B = 0.01$, where (4.2) is satisfied with $D \simeq 0.095$.

region into which C_i is mapped after one period of oscillation is denoted by $F(C_i)$. Then we have

$$D \sim p \sim \mu(F(C_i) \cap C_{i+1})/\mu(C_i). \tag{4.4}$$

To estimate the denominator of (4.4), we suppose that the tori which are not destroyed for $1 \gg B > 0$ do not change their shapes qualitatively from those for $B = 0$. This assumption is assured in terms of the KAM theorem. The z coordinate which separates the chaotic region from the tori at $x = i + 0.5$ is denoted by $z^*(\sim 0.5)$ and the x coordinate which does at $z = 0.0$ is denoted by $x^*(\sim 0)$. The time interval for which the test particles stay near the line $x = 0$ with velocity $u \equiv \dot{x}(t)$ in the x direction is denoted by δt. Then x^* is related to B by $x^* \sim \int_{\delta t} u(0, z(t), t)dt \propto B$ for $B \ll 1$,and z^* is related to x^* by $\Psi_0(x^*, 0) = \Psi_0(0.5, z^*)$. As $|z^* - 0.5| \ll 1$, we have $W(z) \sim (z^* - 0.5)^2$. These equations lead to $|z^* - 0.5| \propto \sqrt{B}$ so that the denominator is estimated as $\mu(C_i) \sim x^* + |z^* - 0.5| \propto B + \sqrt{B}$.

Next we estimate the numerator, which is supposed to be proportional to $< |u| > |z^* - 0.5|$, where $< |u| >$ is the average velocity through the separatrices. The dependence of $< |u| >$ on B is given as follows. By definition,

$$u = -\partial\Psi(x, z, t)/\partial z \sim A \sin\{\pi(x + B \sin(2\pi t))\}(z - 0.5). \tag{4.5}$$

The maximum and minimum value of the probability density $P(z)$ for $z(t)$ in the widespread chaotic region with $z^* < z < 0.5$ between separatrices are denoted by $P_{\max}$ and $P_{\min}$, respectively. If $P_{\max} - P_{\min} \ll P(z)$, then $P(z)$ is

given by $1/(0.5 - z^*)$, leading to

$$< |u| > \sim \int_{z^*}^{0.5} (0.5 - z) P(z) dz \sim (0.5 - z^*) \sim \sqrt{B}. \tag{4.6}$$

After all,

$$D \sim p \propto \frac{< |u| > \sqrt{B}}{B + \sqrt{B}} \sim \sqrt{B}. \tag{4.7}$$

This result differs from that of Solomon and Gollub. Their result can be understood as follows. If one cell is filled uniformly with test particles as in their simulation, then the fact that the particles do not diffuse in tori has to be taken into account. We define the torus region T_i of the ith cell and its area $\mu(T_i)$. Then R_i, T_i and C_i are connected to each other with the relations of $R_i = T_i \cup C_i$ and $T_i \cap C_i = \emptyset$. The diffusion constant in C_i is denoted by D_c and the one in T_i by D_t. $\mu(C_i)$ and D_c are both proportional to $\sqrt{B}$, whereas $\mu(T_i)$ and D_t are proportional to $1 - \sqrt{B}$ and 0, respectively. Then $D = \mu(T_i) \cdot D_t + \mu(C_i) \cdot D_c \sim B$, leading to their linear dependence on B. The diffusion constant, however, should be defined only for chaotic orbits in the widespread chaotic region. Another characteristics of Fig. 4 is to have some fine-grained peaks which are not reported by Solomon and Gollub. Four remarkable peaks are found in Fig. 4 at $B = 0.012$, 0.045, 0.097 and 0.16 as indicated by the arrows. These peaks of D will be referred to as the enhanced diffusion, whose extreme case will lead to accelerator-mode islands in a peak range of B, producing an anomalous diffusion with $D = \infty$. These remarkable features will be characterized by certain structures of the invariant manifolds in fluid space.

5 Accelerator-mode Islands

5.1 Existence of accelerator-mode islands

There exist elliptic periodic points $\{\bar{x}_t, \bar{z}_t\}$ with period Q, on which particles move as

$$|\bar{x}_{t+Q} - \bar{x}_t| = l, \quad \bar{z}_{t+Q} = \bar{z}_t, \quad (t = 1, 2, \cdots, Q) \tag{5.1}$$

with mean speed $v_a = l/Q \leq 1$ for a pair of positive integers l and Q. The Q main islands around $\{\bar{x}_t, \bar{z}_t\}$ are referred to as the accelerator-mode islands with period Q and mean speed $v_a = l/Q$. Indeed we shall show that such accelerator-mode islands appear around the oscillating roll boundaries in a peak range of B. Then there coexist two kinds of islands in the widespread chaotic sea; one is the normal islands with $v_a = 0$, and the other is the accelerator-mode islands with $v_a > 0$. The accelerator-mode islands in a peak range about $B = 0.04$ are investigated below. Indeed two main islands which have $Q = 2$ and $v_a = 1$ appear around points $\{x = \text{integers}, z = 0\}$ in the range $0.039783 < B < 0.041923$, as shown in Fig. 7 for $B = 0.0404$. As shown in Fig. 8 where the rotation number ρ around the periodic points $\{\bar{x}_t, \bar{z}_t\}$ is plotted against B, these islands become unstable at $B = 0.041923$ with eigenvalue -1, where the rotation number becomes $1/2$ in the unit of period two. Then four islands with period four appear, and similar situations continue from 2^n-period to 2^{n+1}-period, leading to a period-doubling tree which has been reported by Greene et al in a two-dimensional map [31]. Figure 9 shows the vertical component of the elliptic periodic points of the

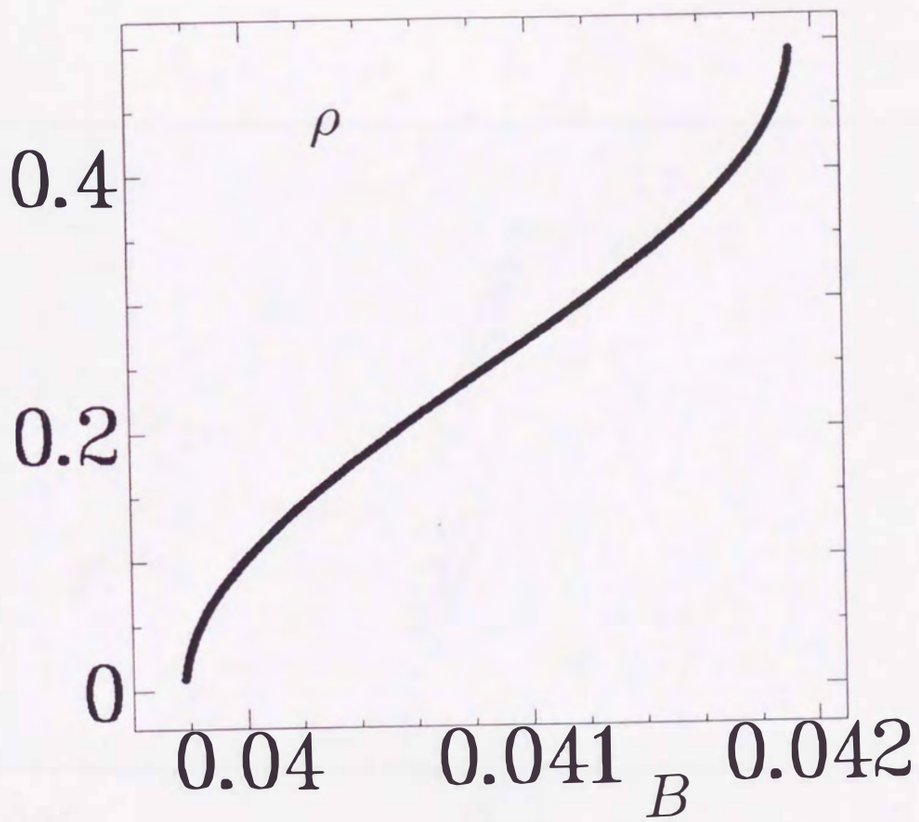

Figure 8: Rotation number ρ of the accelerator-mode islands vs $B(= 0.039783 \sim 0.041923)$, which is obtained from the eigenvalue of the linearized equation of (2.17)

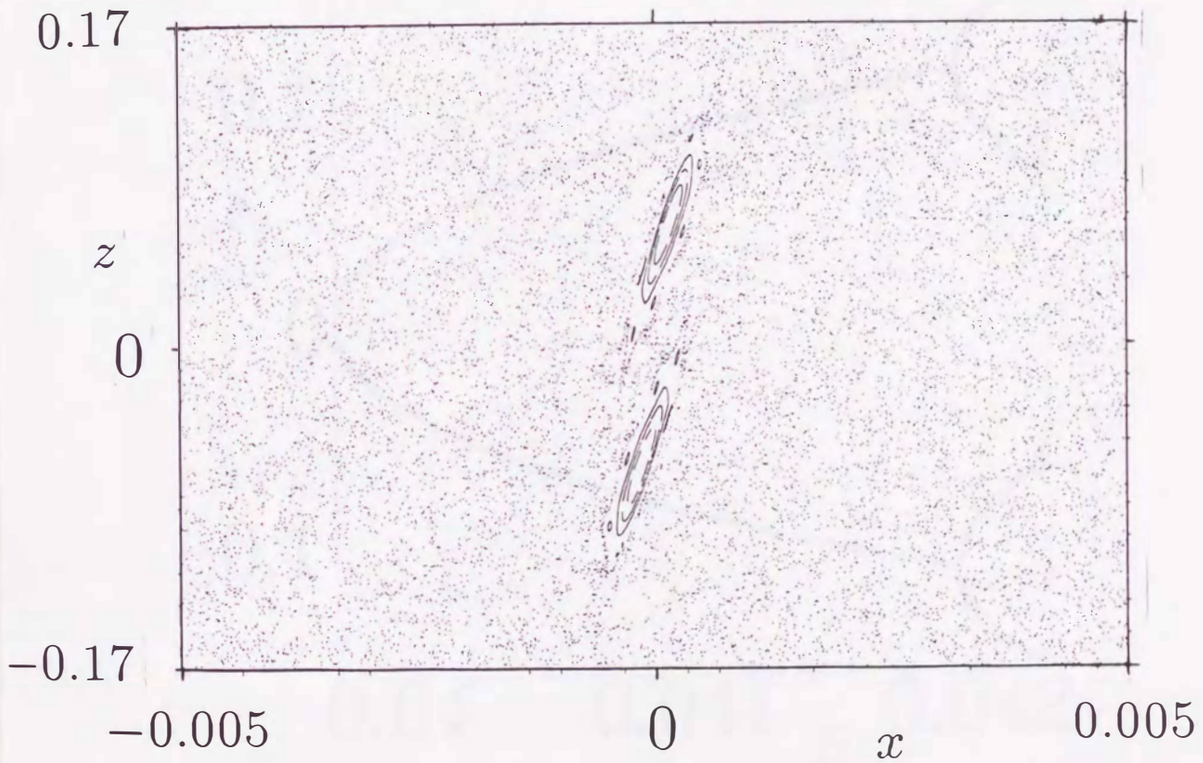

Figure 7: Phase-space portrait of the accelerator-mode islands with $Q = 2$ and $v_a = 1$ for $B = 0.0404$, lying around the roll boundary W_0.

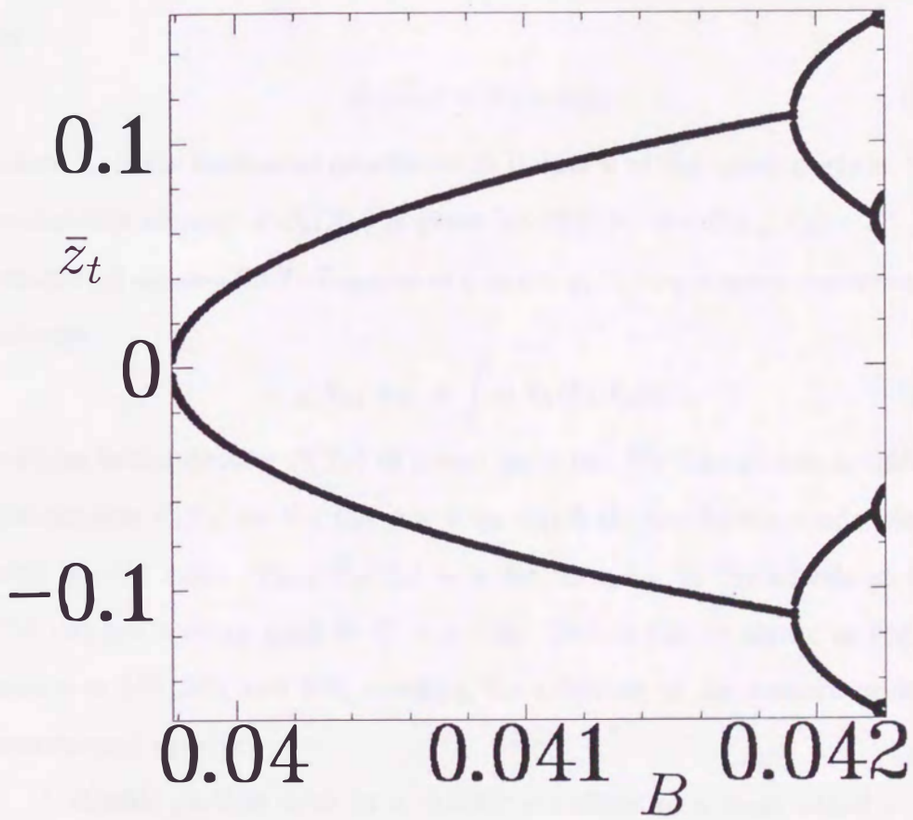

Figure 9: Vertical component $\bar{z}_t$ of the elliptic periodic points vs B. This exhibits the period-doubling tree 2^n from $n = 1$ to $n = 3$.

accelerator-mode islands as a function of B, exhibiting the period-doubling tree from $n = 1$ to $n = 3$.

Indeed Fig. 10 shows the four main islands of period four ($Q = 4$) with $v_a = 1$ at $B = 0.04206$.

The horizontal displacement of a tracer particle for n iterates is denoted by

$$U_n(X_0) = |x_n - x_0|, \tag{5.2}$$

where x_n is the horizontal coordinate at iterate n of the tracer particle. The probability density of $U_n(X_0)$ is given by $P(U;n) \equiv< \delta(U_n(X_0) - U) >_{\rm E}$, where $\delta(g)$ denotes the $\delta-$function of g and $< g(X_0) >_{\rm E}$ denotes the ensemble average

$$< g(X_0) >_{\rm E} \equiv \int g(X_0)P(X_0)dX_0 \tag{5.3}$$

with an initial density $P(X_0)$ of tracer particles. We here choose a uniform distribution $P(X_0)$ on the line $x = 0$ on which the accelerator-mode islands with $v_a = 1$ exist. Then $U_n(X_0) = n$ for X_0 lying on the islands so that $P(U;n)$ has a sharp peak at $U = n$ [32]. This is clearly shown in Fig. 11 with $n = 100$, 200, and 300, ensuring the existence of the accelerator-mode islands with $v_a = 1$.

A chaotic particle orbit in a chaotic sea sticks to a main island in the chaotic sea repeatedly. Hence the island is quantitatively characterized by the distribution function $f(n)$ of sticking times n. A feature of $f(n)$ is the power-law dependence

$$f(n) \propto n^{-1-\beta}, \quad (1 < \beta < 2) \tag{5.4}$$

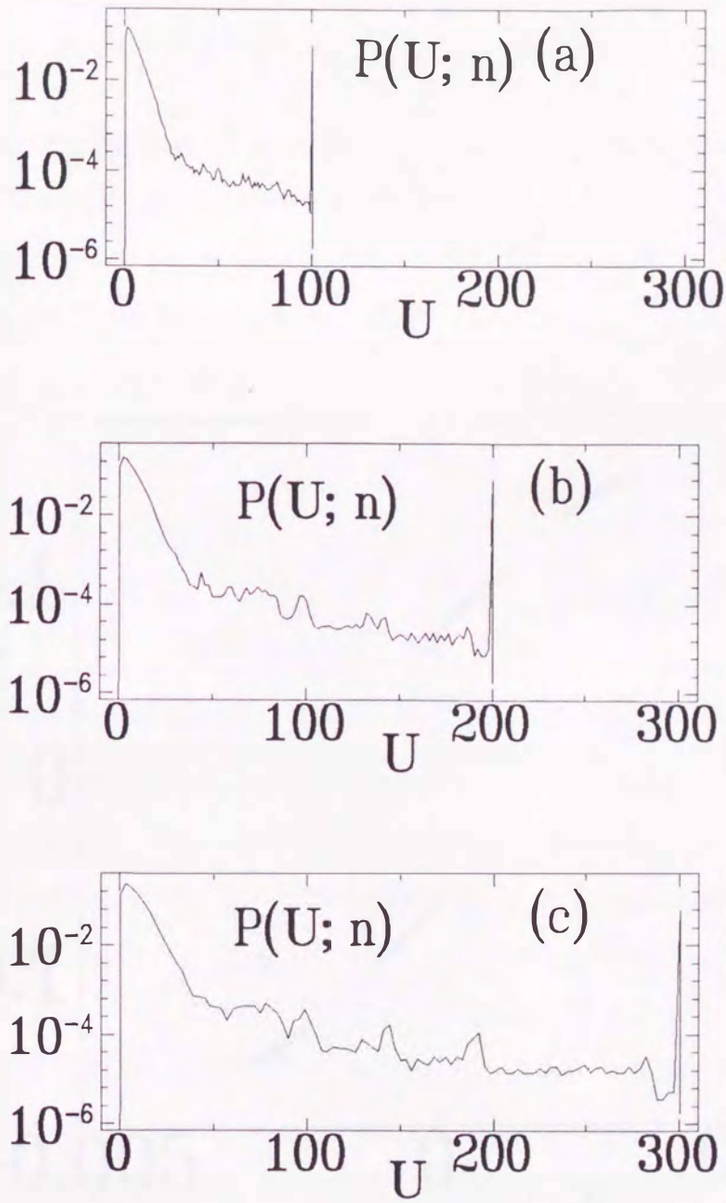

Figure 11: Probability density $P(U;n)$ of $U_n(X_0) = |x_n - x_0|$ for (a) $n = 100$, (b) $n = 200$ and (c) $n = 300$. 100 tracer particles are used for the initial distribution $P(X_0)$ of (5.3).

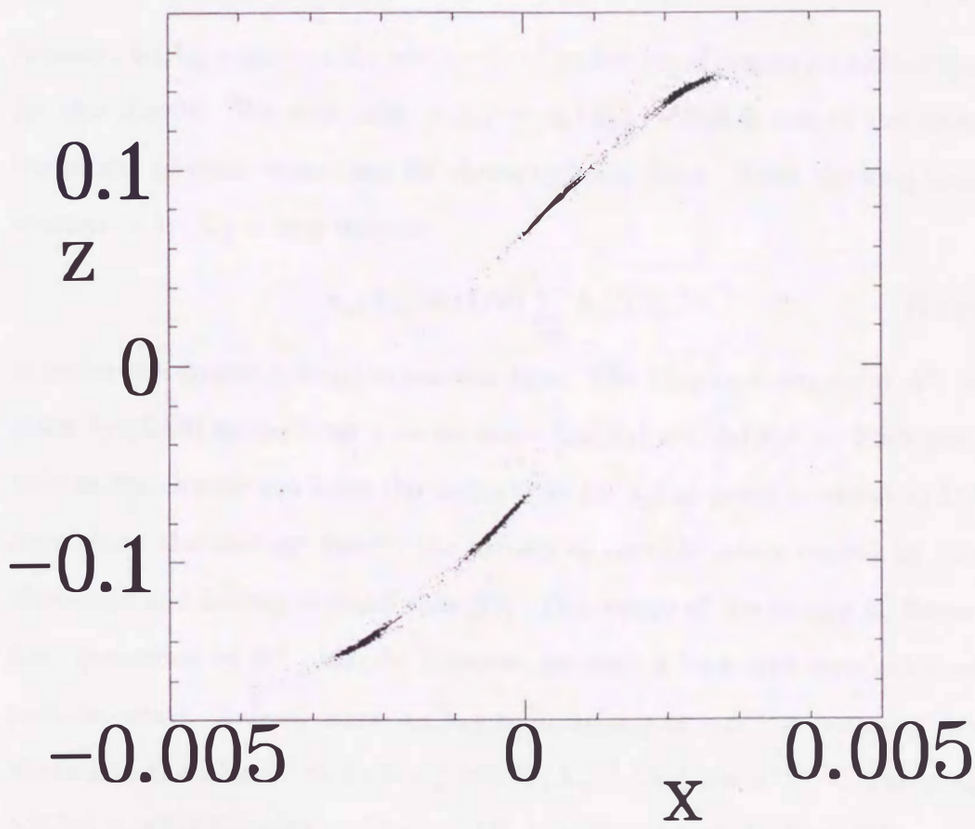

Figure 10: Accelerator-mode islands of period four ($Q = 2^2$) with $v_a = 1$ for $B = 0.04206596$, lying around W_0. Each of the four islands is formed by 300 tracer points.

For a chaotic particle orbit X_t of the map (4.1), let $u_1(X_t)$ be the unit vector tangent to the local unstable manifold at X_t and $DF(X_t)$ be the Jacobian matrix of F at X_t. Then the local expansion rate $\lambda_1(X_t)$ of nearby particle orbits at X_t is defined by [23]

$$\lambda_1(X_t) \equiv \log |DF(X_t)u_1(X_t)|. \tag{5.9}$$

Namely, $\lambda_1(X_t)$ expresses the mean rate of expansion of nearby particle orbits for one iterate. We now take $\omega(X_t) = \lambda_1(X_t)$, which is one of the most important physical quantities for characterizing chaos. Then the long-time average of $\lambda_1(X_t)$ over n iterates,

$$\Lambda_n(X_0) \equiv (1/n) \sum_{t=0}^{n-1} \lambda_1(X_t), \tag{5.10}$$

is called the coarse-grained expansion rate. The Liapunov exponent Λ^∞ is given by (5.10) in the limit $n \to \infty$ since $\Lambda_\infty(X_0) =< \lambda_1(X_0) >$. Each particle in the chaotic sea loses the memory of its initial point in about $1/\Lambda^\infty$ iterates on the average due to the mixing of particle orbits caused by the stretching and folding of small cells [23]. The degree of the mixing is, therefore, quantified by Λ^∞. Islands, however, produce a long-time correlation of particle orbits. Indeed, since $\lambda_1(X_t) \simeq 0$, $\hat{\lambda}_1(X_t) \simeq -\Lambda^\infty \neq 0$ during the sticking to the islands, we have $C_n^\lambda \equiv < \hat{\lambda}_1(X_n)\hat{\lambda}_1(X_0) > \propto n^{-(\beta-1)}$. The sum $S_n^\lambda(X_0) \equiv n\Lambda_n(X_0)$ with $< S_n^\lambda >= n\Lambda^\infty$, therefore, takes the form [34]

$$< (S_n^\lambda - < S_n^\lambda >)^2 >= nC_0^\lambda + 2\sum_{t=1}^{n-1}(n-t)C_t^\lambda \propto n^\zeta \tag{5.11}$$

for large n, where $2 > \zeta = 3 - \beta > 1$. This is in strong contrast to the dissipative dynamical systems for which $1 \geq \zeta \geq 0$ [23]. Indeed Fig. 12

since the particle orbit spends a long time among the hierarchical structure of chains of small islands around the main island repeatedly [33]. The probability that an orbit segment sticks to the island longer than n is given by

$$W(n) \equiv \sum_{t=n}^{\infty} t f(t) \propto n^{-(\beta-1)} \tag{5.5}$$

for large n. Let us apply this to the accelerator-mode islands of speed $v_a = l/Q \neq 0$. Since $U_n(X_0) = nv_a$ during the sticking to the islands, we then have the variance [23]

$$< (x_n - x_0)^2 > \simeq (nv_a)^2 W(n) \propto n^{3-\beta}, \quad (2 > 3-\beta > 1) \tag{5.6}$$

for large n instead of (4.2). Since $3 - \beta > 1$, this leads to the anomalous diffusion where the diffusion constant diverges ($D = \infty$).

5.2 Long-time correlations of particle orbits

Let us take a time series of a physical quantity ω; $\{\omega(X_0), \omega(X_1), \cdots, \omega(X_{N-1})\}$. Then (5.5) leads to the power-law decay of the time-correlation function $C_n^{\omega} \equiv < \hat{\omega}(X_n)\hat{\omega}(X_0) >$ if $\hat{\omega}(X_t) \simeq C \neq 0$ for X_t sticking to the islands, where $\hat{\omega}(X_n) \equiv \omega(X_n) - < \omega(X_0) >$ and $< \cdots >$ denotes the long-time average

$$< G(X_0) > \equiv (1/N) \sum_{t=0}^{N-1} G(X_t) \tag{5.7}$$

with $N \to \infty$. Indeed, C_n^{ω} is estimated as $C_n^{\omega} \simeq C^2 W(n) \propto n^{-(\beta-1)}$. Then the variance of the sum $S_n^{\omega}(X_0) \equiv \sum_{t=0}^{n-1} \omega(X_t)$ takes the form

$$< (S_n^{\omega} - < S_n^{\omega} >)^2 > = nC_0^{\omega} + 2 \sum_{t=1}^{n-1} (n-t) C_t^{\omega} \propto n^{3-\beta}. \tag{5.8}$$

shows the anomalous growth n^{ζ} with $\zeta \simeq 1.37$ for $B = 0.0413782$, leading to $\beta \simeq 1.63$.

There coexist two kinds of islands in the widespread chaotic sea; the accelerator-mode islands with $v_a > 0$ and the normal islands with $v_a = 0$. The anomalous diffusion (5.6) is produced by the accelerator-mode islands, whereas the anomalous mixing (5.11) is produced by any kind of islands. Indeed the anomalous mixing (5.11) with $\zeta \simeq 1.37$ is produced by the coexisting normal islands. It should be noted here that the accelerator-mode islands and the coexisting normal islands produce different values of exponent β, since their neighborhoods have different structures. Then the smaller β determines the variance (5.11), leading to a larger value of ζ, i.e., $\zeta \simeq 1.37$.

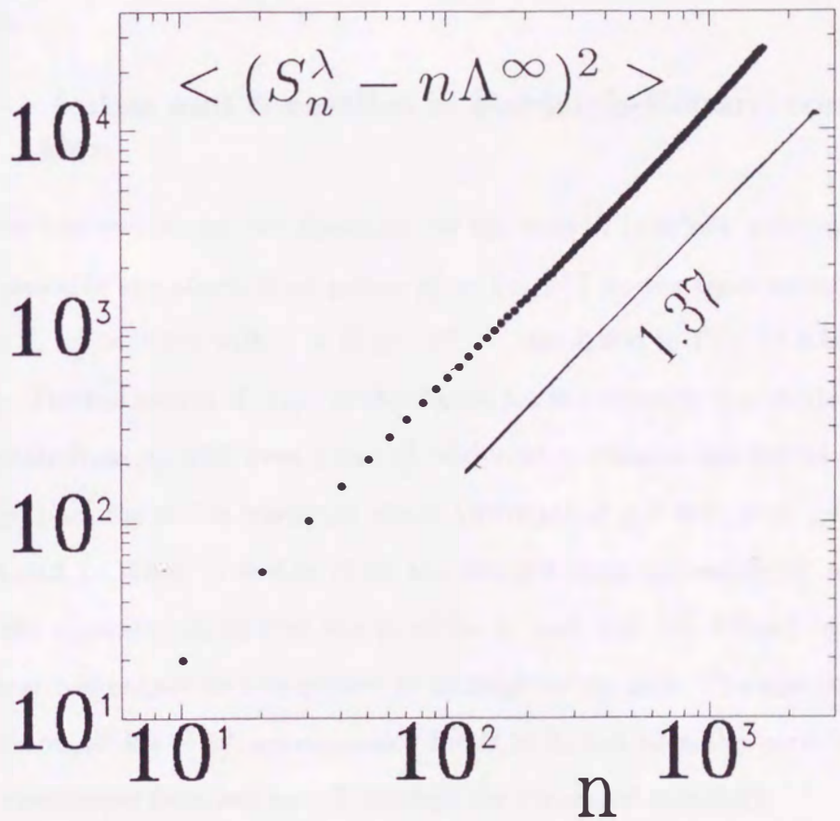

Figure 12: Variance $< (S_n^\lambda - n\Lambda^\infty)^2 >$ vs n ($= 10 \sim 1600$) for $B = 0.0413782$. The length N in the long-time average (5.7) is taken to be 50×10^5. This leads to $\zeta \simeq 1.37$, $\beta \simeq 1.63$.

6 Diffusion and Accelerator-mode Islands in terms of the Lobes

Here we attempt to elucidate and formulate the enhanced diffusion and the accelerator-mode islands from the structures of the unstable and stable manifolds.

6.1 Lobes and turnstiles in Rayleigh-Bénard convection

Let us first review the lobe dynamics for the map (4.1) briefly, starting from the unstable and stable fixed points $p_j^{\pm} \equiv \{x_j, z_j^{\pm}\}$ on the rigid walls, where $x_j = j$, $z_j^{\pm} = \pm 0.5$ with $j = 0, \pm 1, \pm 2, \cdots$, as shown in Fig. 13 schematically. The full curves $W^{\rm u}(p_j^{\mp})$ in this figure are the unstable manifolds which originate from p_j^- with even j and p_j^+ with odd j, whereas the dotted curves $W^{\rm s}(p_j^{\pm})$ are the stable manifolds which terminate at $p_j k$ with even j and p_j^- with odd j. When $B = 0$ in (3.2), the straight lines connecting p_j^+ and p_j^- are the separatrices, so that the particles in each roll cell divided by these separatrices cannot be transported to its neighboring cells. The unstable and stable manifolds of $p_j^{\pm}$ are separated for $B > 0$, and then the particles can be transported from cell to cell through the separated manifolds.

As shown in Fig. 13 (a), we select one principal intersection point (pip) $c_0 \in W^{\rm u}(p_0^-) \cap W^{\rm s}(p_0^+)$ and the line $U[p_0^-, c_0] \cup S[p_0^+, c_0]$ as a pseudo-separatrix W_0, as shown in Fig. 13 (b) [27]. The c_0 is selected so that W_0 resembles the original separatrix of $B = 0$ lying at $x = 0$. As the generalization of c_0, c_j is

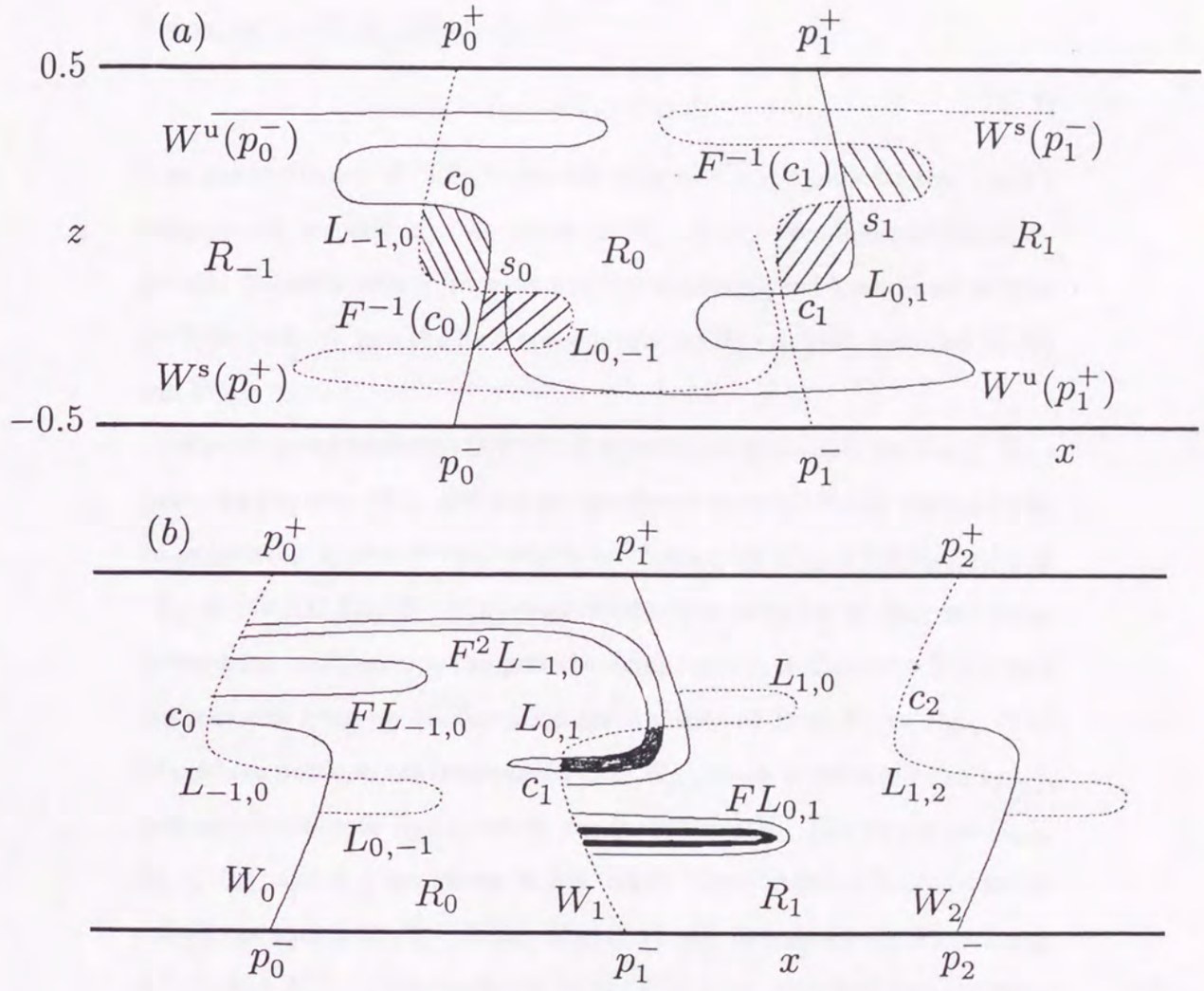

Figure 13: (a) Four invariant manifolds $W^{\mathrm{u}}(p_0^-)$, $W^{\mathrm{s}}(p_0^+)$, $W^{\mathrm{s}}(p_1^-)$, $W^{\mathrm{u}}(p_1^+)$, and pips c_0, s_0, c_1, s_1 are shown with turnstile lobes $L_{-1,0}$, $L_{0,-1}$, $L_{0,1}$, $L_{1,0}$. (b) Pseudo-separatrices W_0, W_1, W_2, and cells R_0, R_1 divided by them are shown with those turnstile lobes $L_{j,j-1}$, $L_{j,j+1}$ with $j = 0, 1$ which lie in R_0 and R_1.The lobes $L_{-1,0}$, $FL_{-1,0}$, $F^2L_{-1,0}$ and $FL_{0,1}$ are also shown schematically.

defined for $j = 0, \pm 1, \pm 2, \cdots$ by

$$(c_{j\pm1})_x = (c_j)_x \pm 1, \quad (c_{j\pm1})_z = -(c_j)_z \tag{4 · 1}$$

from the symmetry of (3.2), where the suffices x and z indicate the x and z components, respectively. As shown in Fig. 13 (b), pseudo-separatrices W_j are also defined similarly, representing the oscillating roll boundaries at time $t = 0, \pm 1, \pm 2, \cdots$, and the fluid space is divided into cells R_j bounded by W_j and W_{j+1}.

$S[F^{-1}(c_j), c_j]$ intersects $U[F^{-1}(c_j), c_j]$ at precisely one pip besides $F^{-1}(c_j)$ and c_j for the map (4.1), and the pip is referred to as s_j. Hence there are two lobes between c_j and $F^{-1}(c_j)$ which are formed by $U[c_j, s_j] \cup S[c_j, s_j]$ and $U[s_j, F^{-1}(c_j)] \cup S[s_j, F^{-1}(c_j)]$, respectively. The particles in R_{j-1} are never transported to R_j except the particles lying on one of these two lobes, and the particles lying on another lobe are transported from R_j to R_{j-1}. The lobe whose particles are transported from R_{j-1} to R_j is referred to as $L_{j-1,j}$, and another lobe as $L_{j,j-1}$, which are turnstiles [35]. The turnstiles $L_{-1,0}$, $L_{0,-1}$, $L_{0,1}$, and $L_{1,0}$ are shown in Fig. 13(a). The turnstiles $L_{j,j\pm1}$ lie in the cell R_j, as shown in Fig. 13 (b). Figure 13 (b) also shows the lobes $L_{-1,0}$, $FL_{-1,0}$ and $F^2L_{-1,0}$ schematically, where $F^2L_{-1,0}$ is stretched over the turnstile $L_{0,1}$ which is mapped into $FL_{0,1}$ in R_1. This indicates how fluid particles are transported from R_0 to $R_{\pm1}, R_{\pm2}, \cdots$ successively through the turnstiles. The turnstiles $L_{j-1,j}$ and $L_{j,j-1}$ lie around the roll boundary W_j, and their dynamics produces the widespread chaotic sea extending over all the cells $R_0, R_{\pm1}, R_{\pm2}, \cdots$. The dynamics of lobes is, therefore, very important for

studying the diffusion of tracer particles from the viewpoint of dynamical systems.

6.2 Elucidation of enhanced diffusion and accelerator-mode islands

We now discuss how the enhanced diffusion and the formation of the accelerator-mode islands can be elucidated in terms of the lobe dynamics. The particles lying in the widespread chaotic region C_0 at $t = 0$ is called the R_0 particles as before. We suppose that the tracer particles are put on the region C_0 uniformly at time $t = 0$, and first derive the concentration of the R_0 particles on C_j, $(j \neq 0)$ after n iterates, $T_j(n) \equiv \mu(C_j \cap F^n C_0)$, in terms of a few lobes and their dynamics. All the regions occupied by those particles which escaped from R_0 for n iterates are given by $\bigcup_{k=1}^{n} F^k(L_{0,1} \cup L_{0,-1})$ in terms of $L_{0,1}$ and $L_{0,-1}$. The particles entering C_j at iterate n must be contained in $L_{j-1,j}$ or $L_{j+1,j}$ at iterate $n-1$. Hence $L^0_{j-1,j}(n) \equiv L_{j-1,j} \cap F^{n-1} C_0$, $(j \neq 0)$ gives a subregion of C_0 which enters C_j at iterate n by passing through $L_{j-1,j}$ at iterate $n-1$, and $\mu(L^0_{j-1,j}(n))$ denotes the amount of the R_0 particles entering C_j at iterate n through $L_{j-1,j}$. Then, using only $4+1$ lobes and their dynamics and applying the formula (2.20), we obtain

$$\mu(L^1_{j-1,j}(n)) = \delta_{j,1}\mu(L_{0,1}) + \sum_{k=1}^{n-1} \sum_{i=\pm 1} [\mu(L_{j-1,j} \cap F^k L_{0,i}) - \mu(L_{j-1,j} \cap F^k L_{i,0})], \tag{6.1}$$

where $\delta_{i,j}$ is the Kronecker δ. The first terms of the summand give the area of the region whose particles once have been on C_0 and enter C_j at iterate

n. Such particles which are not the R_0 particles but entered C_0 from the outside through $L_{1,0}$ or $L_{-1,0}$ have been subtracted by the second terms of the summand. A total flux $J_{j-1,j}(n)$ of the R_0 particles from R_{j-1} to R_j across W_j at iterate n is given by

$$J_{j-1,j}(n) = \mu(L^1_{j-1,j}(n)) - \mu(L^1_{j,j-1}(n)), \tag{6.2}$$

where the first term is a flux from R_{j-1} to R_j and the second is a flux from R_j to R_{j-1}. The particle concentration $T_j(n) = \mu(C_j \cap F^n C_0)$ is related to this $J_{j-1,j}(n)$ by the continuity equation as

$$T_j(n) - T_j(n-1) = J_{j-1,j}(n) + J_{j+1,j}(n). \tag{6.3}$$

Therefore, $T_j(n)$ is easily obtained by integrating this equation as

$$T_j(n) = \sum_{m=1}^{n} \{J_{j-1,j}(m) + J_{j+1,j}(m)\} \quad \text{for } j \neq 1, \tag{6.4}$$

so that $T_j(n)$ can be written only in terms of 8 lobes and their dynamics through (6.2). The region C_0 is given by $C_0 = R_0 \cap \bigcup_{k=0}^{\infty} F^k(L_{0,1} \cup L_{0,-1})$ in terms of the lobes .

Since all the initial points of the tracer particles are put on C_0, the transport probability of the tracer particles from R_j to R_{j+1} at iterate n is given by $J_{j,j+1}(n)/\mu(C_0)$. Let t_B denote the first visit time [27], i.e. , the minimum time in which an appreciable ratio of the R_0 particles is transported from $R_{\pm 1}$ to $R_{\pm 2}$; in other words, the minimum time in which an appreciable amount of the lobes $FL_{0,\pm 1}$ enters the turnstiles $L_{\pm 1,\pm 2}$. Here the translational and time-reversal symmetries of the system have been taken into account. Let τ_B

be the mixing time in which the lobes $F^k L_{0,1}$ and $F^k L_{2,1}$, $(k = 1, 2, \cdots, \tau_B)$ fill C_1 nearly uniformly in a coarse-grained scale so that the initial memory of the lobes $FL_{0,1}$ and $FL_{2,1}$ is lost in τ_B. We may have $t_B \sim \tau_B$ for the normal diffusion outside the peak range of the enhanced diffusion, since the mixing of the lobe $FL_{0,1}$ in C_1 supplies the R_0 particles to the turnstile $L_{1,2}$ through which the transport from R_1 to R_2 occurs. Thus the diffusion of the R_0 particles consists of two processes; one is the mixing of the lobes $FL_{j\mp1,j}$ in C_j to eliminate the initial memory and another is the transport of the R_0 particles from $L_{j\mp1,j}$ to $L_{j,j\pm1}$. The mixing may be related to the intracellular correlation of chaotic particle orbits within one cell, whereas the transport can produce an intercellular correlation of particle orbits between different cells, as can be seen in the case of the enhanced diffusion and the accelerator-mode islands.

Let us first consider the normal diffusion where the mixing dominates over the transport. Then, the flux $J_{\pm j,\pm(j+1)}(n)$ would be locally related to the concentration $T_j(n-1)$ for $j \geq 1$ by

$$J_{\pm j,\pm(j+1)}(n) = -D[T_{\pm(j+1)}(n-1) - T_{\pm j}(n-1)] \tag{6.5}$$

with $n \gg j\tau_B + 1$, which corresponds to Fick's law. Here $n \gg j\tau_B + 1$ is required in order to ensure that the R_0 particles are sufficiently mixed in each C_j so that their spatial distribution within C_j is nearly uniform and their flux $J_{j,j+1}(n)$ is locally determined by $T_j(n-1)$ like (6.5). This is the coarse-graining in space. D can be written as $D = \mu(L_{0,1})/\mu(C_0)$, as will be shown in Appendix. Since $\mu(L_{0,1}) \propto B$ [27] and $\mu(C_0) \propto \sqrt{B}$

case appears in a peak range of B with $B^{\rm e}_{\rm min} < B^{\rm a}_{\rm min} < B < B^{\rm a}_{\rm max} < B^{\rm e}_{\rm max}$. Then it becomes possible that $FL_{j,j+1}$ is stretched over $L_{j+1,j+2}$ so that an appreciable amount of the R_0 particles can move with velocity $v = 1$, leading to $F^j R_0 \cap R_j \neq 0$ for $j \gg 1$, as indicated by Fig. 11. Then the number of cells invaded by the R_0 particles grows linearly in time [26, 27], and those particles which invade cells infinitely are the particles lying in the accelerator-mode islands. The number of cells invaded by other than these particles grows as n^α with $1 > \alpha = (3 - \beta)/2 > 0.5$, as indicated by (5.6).

As discussed above, the stretching of the lobe $FL_{j,j+1}$ over the turnstile $L_{j+1,j+2}$ in a few iterates is possible in various ways, so that various fine peaks of D and accelerator-mode islands can appear as B is changed. The situation may be similar to the standard map [32].

Let $A^\pm_j$ denote all the regions of the accelerator-mode islands in C_j so that the particles lying in $A^\pm_0$ are transported to $x = \pm\infty$ with definite velocity $\pm v_a$ through the turnstiles $L_{j,j\pm1}$, $(j = 0, \pm1, \pm2, \cdots)$. Further let us write as

$$\sigma \equiv 1/v_a = Q/l = q/p \geq 1, \tag{6.6}$$

where $p = 1$ if σ is an integer and q/p is a reduced fraction otherwise. Then we have

$$A^\pm_{pi} = F^{\pm qi} A^\pm_0, \quad (i = 0, \pm1, \pm2, \cdots); \tag{6.7}$$

namely, q iterates give a displacement of $A^\pm_j$ in j by p. If $v_a = 1$, then $p = q = 1$, $A^\pm_j = F^{\pm j} A^\pm_0 \subset L_{j,j\pm1}$. If $v_a = 2/3$, then $p = 2$, $q = 3$, $A^\pm_{2i} = F^{\pm 3i} A^\pm_0$. In general, at least one of the Q main islands of $A^\pm_j$ must lie

, as shown previously [21], this leads to $D \propto \sqrt{B}$ in agreement with the statistical-mechanical definition of D by (6.3). Then the number of cells invaded by the R_0 particles grows like $n^{1/2}$. Applying (6.4) and (6.5) to $[T_j(n+t_B)-T_j(n)]/t_B$ and replacing it by $\partial T_j(n)/\partial n$, we obtain the diffusion equation $\partial T_j(n)/\partial n = D\partial^2 T_j(n)/\partial j^2$ in the limit $t_B/n \to 0$, where $j \gg 1$, $n \gg 1$. This leads to the Gaussian distribution $T_j(n) \propto n^{-1/2}\exp(-j^2/4Dn)$.

When B is in the peak range of the enhanced diffusion with $B^{\rm e}_{\rm min} < B < B^{\rm e}_{\rm max}$, the lobe $FL_{0,1}$ is stretched over the turnstile $L_{1,2}$ in a few iterates similarly to Fig. 13 (b), so that the first visit time t_B becomes small with $t_B \ll \tau_B$ and the transport of the R_0 particles from R_1 to R_2 becomes large [21]. Such a coherent transport from R_{j+1} to R_{j+2} occurs over several cells, say, up to $j = j_T$. After that, however, the R_0 particles lying on the lobe $FL_{j,j+1}$ become very small, being supplied only by the mixing in the preceding cells, so that many repetitions of the transport from R_{j+1} to R_{j+2} through $L_{j+1,j+2}$ are needed to transport an appreciable amount of the R_0 particles. This leads to a diffusion process. Then $(4 \cdot 6)$ would also be valid for $j > j_T > 1$ with $D = (\tau_B/t_B)D_m$ and $D_m \equiv \mu(L_{0,1})/\mu(C_0)$, leading to the peaks of D in Fig. 4.

We next examine the formation of the accelerator-mode islands. As an extreme case of the enhanced diffusion, let us consider the limit $j_T \to \infty$ where the coherent transport of an appreciable amount of the R_0 particles from R_{j+1} to R_{j+2} by the stretching of the lobe $FL_{j,j+1}$ over $L_{j+1,j+2}$ in a few iterates occurs over all the cells $j = 0 \sim \infty$. Indeed such an extreme

in $L_{j,j\pm1}$. If $v_a \neq 1$ so that $p < q$, however, at least one of the Q main islands must lie outside $L_{j,j\pm1}$. Furthermore we have $R_0 \cap F^{\mp qi} R_{pi} \neq 0$ and

$$A_0^{\pm} = \bigcap_{i=0}^{\infty} F^{\mp qi} R_{pi} = \bigcap_{i=0}^{\infty} F^{\pm qi} R_{-pi}, \tag{6.8}$$

where, if $v_a = 1$, then R_{pi}, R_{-pi} can be replaced by $L_{i,i\pm1}$, $L_{-i,-i\pm1}$, respectively. Equation (6.8) represents the limit of the coherent transport. Thus the cell R_0 contains a region A_0^+ with a nonzero area $\mu(A_0^+)$ whose particles pass through $L_{j,j+1}$, $(j = 0, 1, 2, \cdots)$ successively and do move to $+\infty$ with a definite velocity. This is the accelerator-mode islands described in terms of the lobe dynamics. Thus, we obtain

Lemma: accelerator-mode islands with $v_a = 1$ must exist in the turnstiles $L_{j,j\pm1}$, $(j = 0, \pm1, \pm2, \cdots)$ for the peak range of B.

Figure 14 shows the accelerator-mode islands with $Q = 2$ and $v_a = 1$ at $B = 0.0404411$, lying in $L_{-1,0}$, $L_{0,1}$ and $L_{1,2}$, and four invariant manifolds $W^{\mathrm{u}}(p_0^-)$, $W^{\mathrm{s}}(p_0^+)$, $W^{\mathrm{u}}(p_2^-)$, $W^{\mathrm{s}}(p_2^+)$. It is also shown that $A_j^+ \subset L_{j,j+1}$ with $j = -1$, 0, 1. $FL_{-1,0}$ and $F^{-1}L_{1,2}$ are stretched over $L_{0,1}$, justifying $A_0^+ \subset FL_{-1,0} \cap F^{-1}L_{1,2}$. It may easily be understood that $A_0^+ = \lim_{j\to\infty} F^j L_{-j,-(j-1)} \cap F^{-j} L_{j,j+1}$.

6.3 Long-time correlation due to accelerator-mode islands

Finally we consider the chaos border in the neighborhood of $A_j^{\pm}$, and relate the lobe dynamics to (5.5) or the exponent β. Hereafter we pay attention to

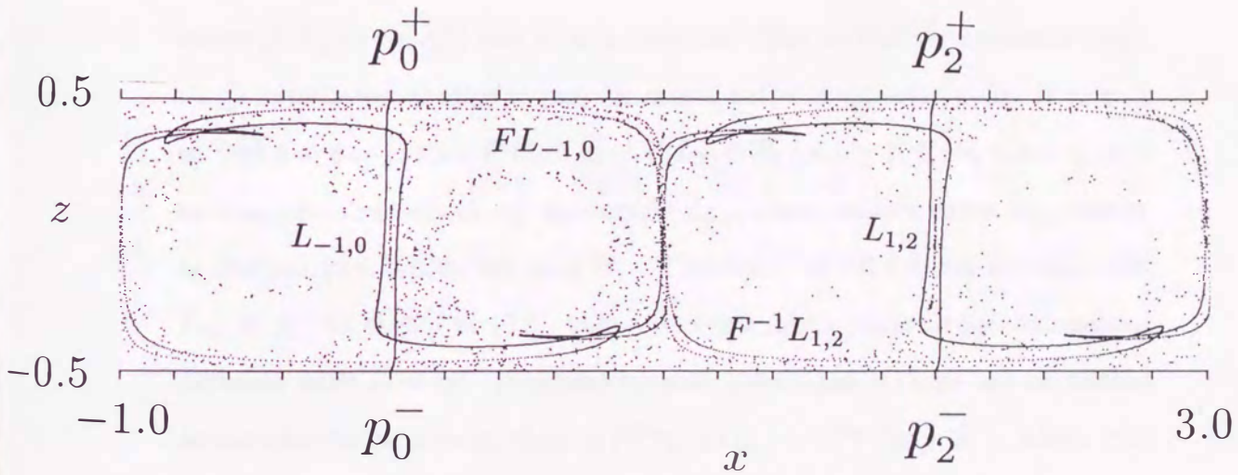

Figure 14: Accelerator-mode islands with $Q = 2$ and $v_a = 1$, lying in the lobes $L_{-1,0}$, $L_{0,1}$ and $L_{1,2}$ around the roll boundaries, and four invariant manifolds $W^{\mathrm{u}}(p_0^-)$, $W^{\mathrm{s}}(p_0^+)$, $W^{\mathrm{u}}(p_2^-)$ and $W^{\mathrm{s}}(p_2^+)$. $W^{\mathrm{u}}(p_0^-)$ is obtained by putting 5000 tracer particles uniformly from p_0^- along $W^{\mathrm{u}}(p_0^-)$, and iterating 7 times. $L_{0,1}$ lies at $x = 1.0$ with shape similar to $L_{-1,0}$. This justifies $A_0^+ \subset FL_{-1,0} \cap F^{-1}L_{1,2}$ and the Lemma.

the islands A_{pi}^{+} with mean velocity $v_a = p/q$ which are characterized by

$$F^{qi}C_0 \cap R_{pi} \to A_{pi}^{+} \quad \text{for} \quad i \to \infty. \tag{6.9}$$

The chaotic R_0 particles which lie outside A_0^{+} but stick to A_{pi}^{+} longer than qi also contribute to $F^{qi}C_0 \cap R_{pi}$, so that (5.5) leads to the power-law decay

$$\mu(F^{qi}C_0 \cap R_{pi}) = \mu(A_0^{+}) + C(qi)^{-(\beta-1)} \quad \text{for} \quad i \to \infty, \tag{6.10}$$

where $\mu(A_{pi}^{+}) = \mu(A_0^{+})$ and C is a constant. The second term gives a long-range correlation of chaotic particle orbits between different cells. If $v_a = 1$ so that $p = q = 1$, then $F^i C_0 \cap R_i = F^i L_{0,1} \cap R_i$ for $i \geq 1$. Even when $v_a \neq 1$ so that some islands of A_0^{+} lie outside $L_{0,1}$, these islands enter $L_{0,1}$ within Q iterates just before entering R_1. Therefore, (6.10) relates the turnstile $L_{0,1}$ to β. As shown in (5.6), this power-law decay leads to the anomalous diffusion with $D = \infty$. It should be also noted that if there are no visible accelerator-mode islands, then $\mu(F^{jt_B} C_0 \cap R_j) \propto r^{jt_B}$ for $j \gg 1$, where r is a number less than unity.

The neighborhood of the main islands around the periodic points $(\bar{x}_t, \bar{z}_t)$ has a hierarchical structure of chains of small islands [33]. Chaotic particles sticked to the main islands are trapped by this structure and spend long times before the escape from the neighborhood, leading to the power-law decay (6.10). Each of A_j^{+} contains such a hierarchical structure of chains of small islands. In order to characterize this hierarchical structure of islands more directly, we introduce the measure

$$m_\sigma(i) \equiv \mu(\bigcup_{k=0}^{i} F^{q(i-k)} R_{-p(i-k)} \cap F^{-qk} R_{pk}), \tag{6.11}$$

where $R_0 \cap F^{-qk} R_{pk} \neq 0$. Here $F^{q(i-k)} R_{-p(i-k)} \cap F^{-qk} R_{pk}$ means the region of A_0^+ and its neighborhood whose particles are trapped at least by A_{pj}^+'s with $j = -(i-k), -(i-k)+1, \cdots, k$, successively. Hence $\Delta m_\sigma(i) \equiv m_\sigma(i) - \mu(A_0^+)$ means the measure of the region around these islands whose particles stick to the islands at least for qi iterates. Hence (5.5) leads to $\Delta m_\sigma(i) \propto (qi)^{-(\beta-1)}$ for $i \to \infty$ in agreement with (6.10). The measure of a chaos-border region, whose particles stick to the islands just for qi iterates and then escape inside the chaotic sea, is given by

$$\delta m_\sigma(i) \equiv m_\sigma(i) - m_\sigma(i+1). \tag{6.12}$$

In order to study the hierarchical structure of the chaos border, we have to take $i \to \infty$. Then $\delta m_\sigma(i) \propto i^{-\beta}$ for $i \to \infty$. If $v_a = 1$ so that $p = q = 1$, then R_{pk} can be replaced by $L_{k,k+1}$ and (6.11) can be written as

$$\begin{aligned} m_\sigma(j) &= \mu\{\bigcup_{k=0}^{j} F^{(j-k)} L_{k-j,k-j+1} \cap F^{-k} L_{k,k+1}\}, \\ &= \mu\{\bigcup_{k=0}^{j} t_k[F^{-k}(F^j L_{-j,-j+1} \cap L_{0,1})]\} \end{aligned} \tag{6.13}$$

with $t_k[\Re] = \{(x,z) | (x_0, z) \in \Re, x = x_0 + k, k \in Z\}$. Then only two lobes and their dynamics are required to determine $m_\sigma(j)$ for $j \to \infty$. It should be also noted that the result $\delta m_\sigma(j) \propto j^{-\beta}$ for the chaos border gives the minimum value of β with $\beta > 1$, because if $\beta = 1$, then the area of the chaos border diverges as $\sum_{j\sim 1}^{\infty} \delta m_\sigma(j) \sim \lim_{j\to\infty} \log j = \infty$.

7 Distribution of Coarse-grained Expansion Rates and its Anomalous Scaling

In § 6, we have noted that a particle orbit in the chaotic sea loses the memory of its initial point in about τ_B iterates due to the mixing of particle orbits caused by the stretching and folding of the lobes, but the intermittent sticking to islands causes the long-time correlation $C_t^{\lambda} =< \hat{\lambda}_1(X_t)\hat{\lambda}_1(X_0) > \propto t^{-(\beta-1)}$, $(2 > \beta > 1)$. This suggests that the probability density of $\Lambda_n(X_0)$ defined by

$$P(\Lambda; n) \equiv < \delta(\Lambda_n(X_0) - \Lambda) > \tag{7.1}$$

is different from the Gaussian distribution, since the sum (5.10) does not satisfy the central limit theorem. It is related to the exponent $\zeta \simeq 1.37$ of the anomalous mixing (5.11). Indeed the Gaussian distribution is not valid for the hamiltonian dynamical systems with a few degrees-of-freedom, since they have the long-time correlation and the tangency points of the unstable and stable manifolds. Then it is convenient to introduce the expansion-rate spectrum [23]

$$\psi_n(\Lambda) \equiv -(1/n)\log\{P(\Lambda; n)/P(\Lambda^{\infty}; n)\} \tag{7.2}$$

for large n, which may be assumed to become independent of n as $n \to \infty$. The $\psi_{\infty}(\Lambda)$ is a concave function of Λ with minimum value $\psi_{\infty}(\Lambda^{\infty}) = 0$. Figure 15 shows $\psi_n(\Lambda)$ with n = 100, 200, 400, 800 and 1600 at B = 0.0413782, where the length N in the long-time average (5.7) is taken to be 2×10^7. This figure reveals that in the limit $n \to \infty$ $\psi_n(\Lambda) = 0$ for

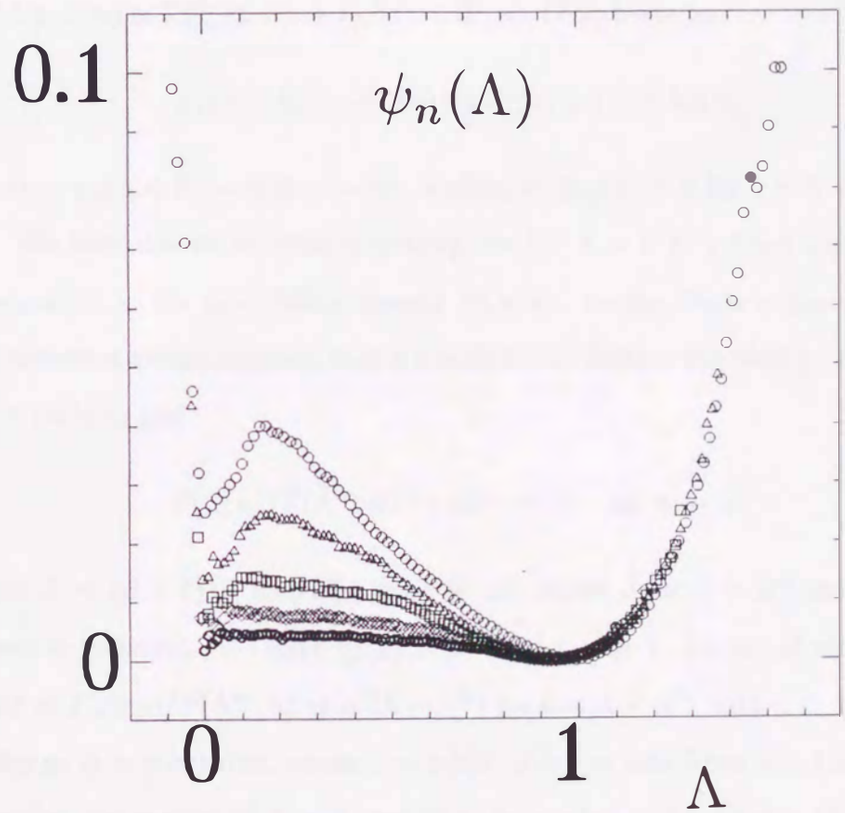

Figure 15: Expansion-rate spectrum $\psi_n(\Lambda)$ for $B = 0.0413782$, where five plots for $n = 100, 200, 400, 800, 1600$ are shown with $N = 5 \times 10^5$. We have $\Lambda^\infty \simeq 0.919$. Two linear parts with slope 0 and -2 are visible as n increases.

$0 < \Lambda < \Lambda^\infty$ and $\psi_n(\Lambda) \propto (\Lambda - \Lambda^\infty)^{1/\delta}$, $1/\delta > 2$ for $\Lambda > \Lambda^\infty$ [21, 34]. This feature of $\psi_\infty(\Lambda)$ for $\Lambda > 0$ comes from the long-time correlation of C_t^λ noted above. Indeed the fact that $\psi_\infty(\Lambda) = 0$ for $0 < \Lambda < \Lambda^\infty$ comes from the orbits X_t sticking to the islands for long times, where $\Lambda_n(X_t) \simeq 0$. Since $P(\Lambda \simeq 0; n) \propto \sum_{t=n}^\infty (t - n + 1) f(t) = W(n)$, (7.2) leads to

$$\psi_n(\Lambda \simeq 0) \propto -(1/n) \log W(n) \propto (1/n) \log n, \tag{7.3}$$

so that $\psi_n(\Lambda \simeq 0) \to 0$ as $n \to \infty$, leading to $\psi_\infty(\Lambda) = 0$ for $0 < \Lambda < \Lambda^\infty$.

We then use an anomalous scaling law for $\Lambda > 0$ to extract further information on the probability density $P(\Lambda; n)$. Indeed Feller's theorem [37] of recurrent events suggests that a rescaled distribution function $g_\beta(x)$ exists and leads to [38]

$$P(\Lambda; n)/P(\Lambda^\infty; n) \to g_\beta(-cn^\delta \hat{\Lambda}) \quad \text{as} \quad n \to \infty \tag{7.4}$$

with $\delta = (\beta - 1)/\beta$ and $P(\Lambda^\infty; n) \sim n^\delta$, where $\hat{\Lambda} \equiv \Lambda - \Lambda^\infty$ and c is a positive constant. We have $g_\beta(x) \propto x^{-\beta-1}$ for $x \gg 1$. Figure 16 shows the plot of $P(\Lambda; n)/P(\Lambda^\infty; n)$ vs $n^\delta |\Lambda - \Lambda^\infty|$ for $0 < \Lambda < \Lambda^\infty$ with $n = 400$, 800, 1600 at $B = 0.0413782$, where $\delta = 0.387$, $\beta + 1 = 2.63$ from $\beta = 1.63$. This justifies the scaling (7.4) and captures the weaker n-dependence of $P(\Lambda; n)$ to complement $\psi_\infty(\Lambda) = 0$ for $0 < \Lambda < \Lambda^\infty$.

For $\Lambda > \Lambda^\infty$, (7.4) leads to $g_\beta(x) \propto \exp[-|x|^{1/\delta}]$ for $-x \gg 1$ [39]. This leads to [38]

$$\psi_n(\Lambda) \propto (\Lambda - \Lambda^\infty)^{1/\delta} \quad \text{for} \quad 0 < \Lambda - \Lambda^\infty \ll \Lambda^\infty, \tag{7.5}$$

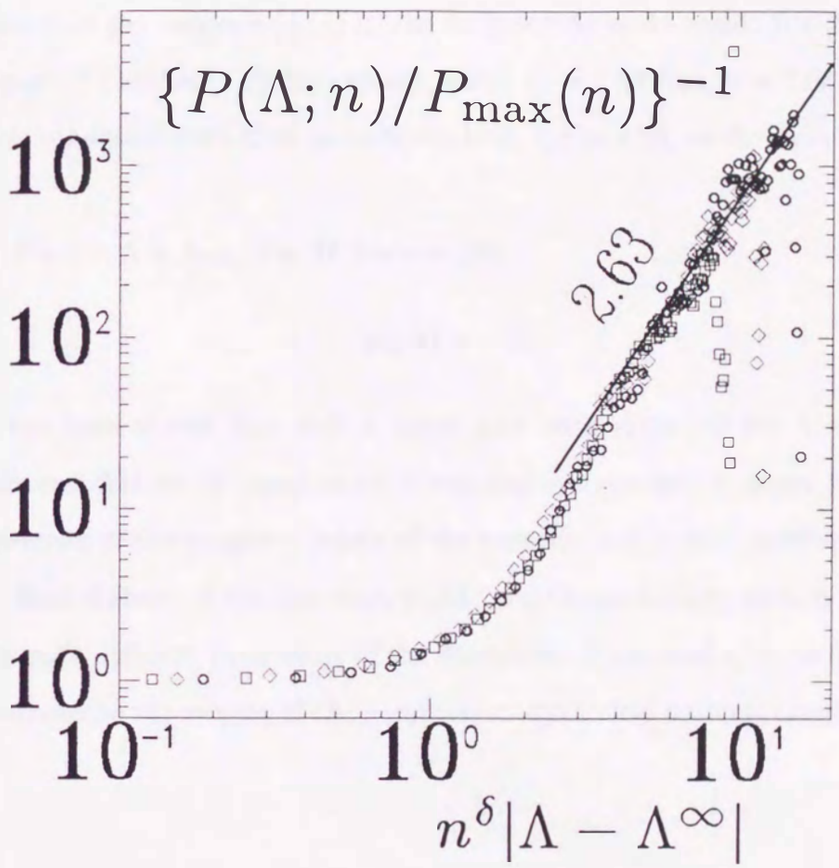

Figure 16: $\{P(\Lambda;n)/P_{\max}(n)\}^{-1}$ vs $n^\delta|\Lambda-\Lambda^\infty|$ for $B=0.0413782$ with $\delta=0.387$, where three plots for $n=400,800,1600$ are shown with $N=5\times10^5$. This justifies the asymptotic form (7.4) with exponent $\beta+1=2.63$.

$$< \theta(S_n^\lambda - n\Lambda^\infty)(S_n^\lambda - n\Lambda^\infty)^2 > \propto n^{\zeta_+}, \quad (\zeta_+ = 2/\beta) \tag{7.6}$$

where $\theta(x)$ is the step function taking 1 for $x > 0$ and 0 for $x < 0$, and $\zeta_+ = 2(1-\delta) = 2/\beta$. Since $2/\beta < \zeta = 3 - \beta$, the conditional variance (7.6) is masked in the variance (5.11) by the fluctuations in the region $0 < \Lambda < \Lambda^\infty$. Figure 17 justifies (7.6) numerically, where $\zeta_+ = 1.23$ from $\beta = 1.63$. Figure 15 is consistent with (7.5) numerically with $1/\delta \simeq 2.58$, as shown in Fig. 18.

For $0 > \Lambda > \Lambda_{\min}$, Fig. 15 leads to [38]

$$\psi_n(\Lambda) = -2\Lambda. \tag{7.7}$$

It has been shown that such a linear part with slope -2 for $\Lambda < 0$ is a universal feature of hamiltonian dynamical systems which arises from the dynamics of the tangency points of the unstable and stable manifolds.

Such features of the spectrum $\psi_\infty(\Lambda)$ and the probability density $P(\Lambda; n)$ are quite different from those of the dissipative dynamical systems [23], and characterize the mixing of the hamiltonian dynamical systems clearly.

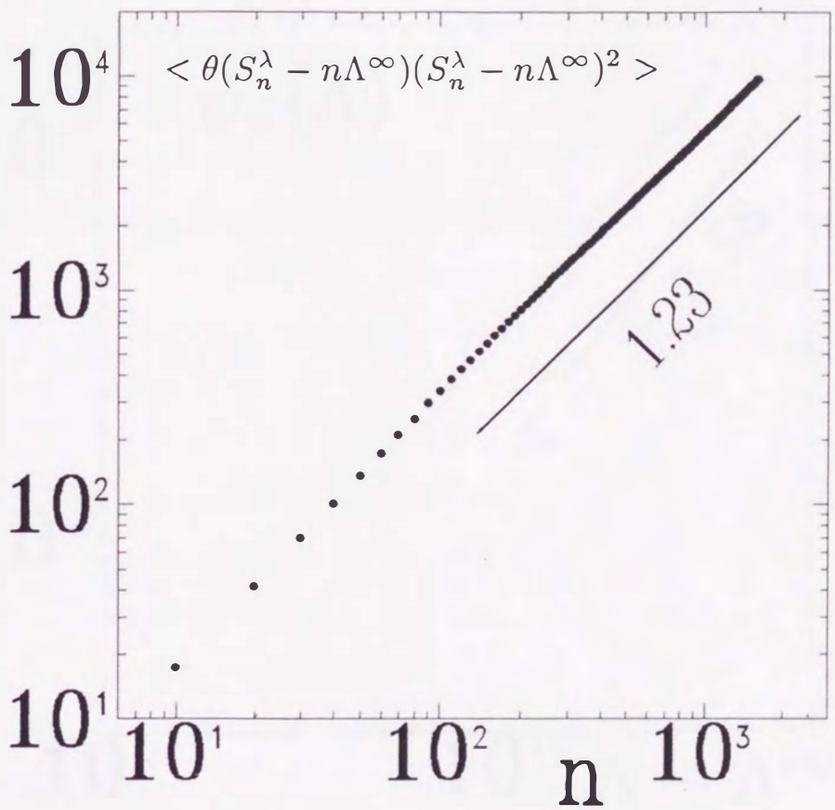

Figure 17: $< \theta(S_n^\lambda - n\Lambda^\infty)(S_n^\lambda - n\Lambda^\infty)^2 >$ vs n $(= 10 \sim 1600)$ for $B = 0.0413782$ with $N = 5 \times 10^5$. This justifies (7.6) with $\zeta_+ = 2/\beta = 1.23$ and $\beta = 1.63$.

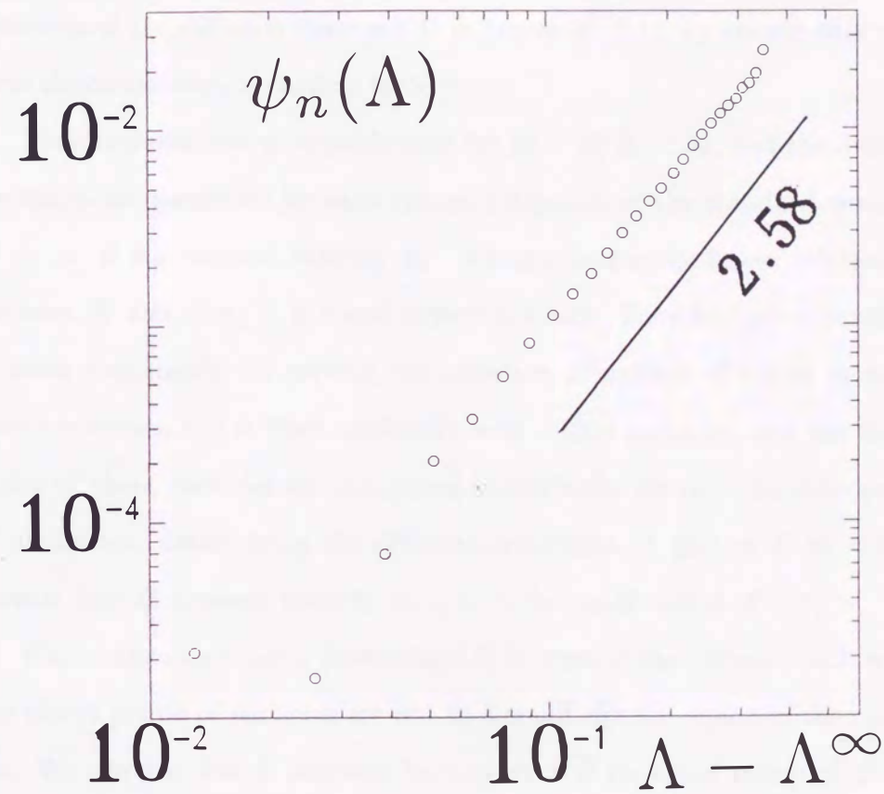

Figure 18: $\log \psi_n(\Lambda)$ vs $\log(\Lambda - \Lambda^\infty)$ for $\Lambda > \Lambda^\infty$ with $n = 800$, $N = 5 \times 10^5$, where the slope agrees with $1/\delta = 2.58$.

8 Summary

In this paper we have discussed anomalous behaviors of tracer particles and stable accelerator-mode islands in an oscillating laminar Rayleigh-Bénard convection, and we compared with Solomon and Gollub's experiments. They determined the diffusion constant D in terms of (3.1), by taking only short time characteristics of particle trajectories.

Their experiments were performed for $19 < R/R_c < 32$, and the diffusion constants are measured for each run as a function of the standard deviation $< \sigma_v >$ of the vertical velocity v_z. An approximately linear relationship between D and $< \sigma_v >$ is found experimentally. They further ensured the relation numerically by solving the equation of motion of tracer particles. One convection roll is filled uniformly with 10000 particles, and the trajectories of these particles are computed individually for one complete period of oscillation, determining the diffusion constants. A plot of D vs $< \sigma_v >$ reveals that D depends linearly on $< \sigma_v >$ for small values of $< \sigma_v >$.

We, on the other hand, determined D in term of the variance (4.2) where the initial points of particles are put in a small chaotic region of the chaotic sea. We can see that D depends linearly on $\sqrt{B}$ for small values of B with several fine-grained peaks. The dependence $D \propto \sqrt{B}$ is different from that of Solomon and Gollub's, which comes from that the area of the torus region $\mu(T_i)$ depends on B. The peaks are due to an interceller correlation of particle orbits between different roll cells. In the peak range of B there exists stable accelerator-mode islands around the roll boundaries, leading to

an anomalous diffusion of tracer particles where the diffusion constant determined from (4.2) diverges. These islands exhibit even period doubling. Where the accelerator-mode islands exist, the statistical properties of the coarse-grained horizontal velocity $v_n(X_0) = (x_n - x_0)/n$ is characterized by the intermittent sticking of tracer particles to the islands through the long-time correlation of particle orbits $C_n \propto n^{-(\beta-1)}$, $(1 < \beta < 2)$. The probability density $P(v;n) \equiv < \delta(v_n(X_0) - v) >$ must obey the anomalous scaling law [25]

$$P(v;n) = n^{\delta}\hat{p}(n^{\delta}v) \quad \text{for } n \gg 1 \tag{8.1}$$

with $\delta = (\beta - 1)/\beta < 1/2$, where $\hat{p}(x)$ is an even function of x and decays as $|x|^{-(1+\beta)}$ for $|x| \gg 1$. However, we could not succeed in obtaining the result of the anomalous diffusion numerically, because of too small tracer particles in our simulation. If their number is increased much more, or experiments are performed for real fluids where the number of tracer particles is $N \sim 10^{23}$, then the anomalous diffusion will be observed.

We then attempted to elucidate and formulate the diffusion of fluid particles, including the enhanced diffusion and the formation mechanism of the accelerator-mode islands from the structures of unstable and stable manifolds. The accelerator-mode islands $A_0^{\pm}$ in C_0 and the area of the region around these islands whose particles stick to the islands just for i iterates are obtained in terms of the turnstiles and their dynamics in the case $v_a = 1$. We have revealed that the unstable and stable manifolds are infinitely accumulated around the accelerator-mode islands.

The mixing in a widespread chaotic sea is characterized in terms of the spectrum $\psi(\Lambda)$ and the probability density $P(\Lambda;n)$ of the coarse-grained expansion rates Λ_n of nearby particle orbits. The spectrum $\psi_\infty(\Lambda)$, defined by (7.2), has two linear parts with slope zero for $0 < \Lambda < \Lambda^\infty$ and slope -2 for $0 > \Lambda > \Lambda_{\min}$. The slope zero is produced by the long-time correlation of particle orbits due to the intermittent sticking to islands, whereas the slope -2 is caused by the dynamics of the tangency points of the unstable and stable manifolds. Then the probability density $P(\Lambda;n)$ for $\Lambda > 0$ obeys an anomalous scaling law $P(\Lambda;n) = n^\delta p(n^\delta \hat{\Lambda})$ for $n \gg 1$ with $\delta = (\beta-1)/\beta < 1/2$, $\hat{\Lambda} \equiv \Lambda - \Lambda^\infty$, where $p(x)$ decays as $|x|^{-(1+\beta)}$ for $-x \gg 1$ and $\exp[-ax^{1/\delta}]$, $(a > 0)$ for $x \gg 1$. This is due to the coexisting normal islands so that the value of δ is different from that of δ in (8.1). These remarkable features of the mixing have been justified for the oscillating Rayleigh-Bénard flow numerically.

The results of § 5 and § 7 have been found also for the standard map.[25, 34, 38] Therefore, it turns out that these results give the universal features which are generally valid for the widespread Lagrangian turbulence of fluids as well as the widespread chaos of the two-dimensional periodic maps such as the standard map, and they can be formulated in terms of the lobe dynamics from the viewpoint of dynamical systems.

Acknowledgments

I would like express my sincere gratitude to Prof. H. Mori and Prof. H. Fujisaka for their encouragements and valuable discussions. I am very glad to have been collaborating with Prof. H. Mori, Prof. H. Fujisaka, Dr. T. Horita, Dr. N. Mori and Mr. K. Egami in this study. I would like to thank them as well as Prof. H. Okamoto, Prof. T. Yoshida, Dr. H. Hata and Dr. T. Kobayashi and all other members of our chaos group at Kyushu University for valuable advice and suggestion. æ

Appendix A

$D = \mu(L_{0,1})/\mu(C_0)$ for the Diffusion Constant

Using (6.2), we rewrite (6.5) as

$$\mu(L^0_{j,j+1}(n)) - \mu(L^0_{j+1,j}(n)) = D[T_j(n-1) - T_{j+1}(n-1)] \tag{A.1}$$

for $j \geq 1$, $j > j_T$, where $n \gg j\tau_B + 1$.

First consider $L^0_{j,j+1}(n) = L_{j,j+1} \cap F^{n-1}C_0$ introduced just above (6.1). The R_0 particles which lie on $L_{j,j+1}$ at iterate $n-1$ must pass through $L_{j-1,j}$ until $t = n-2$. Therefore we may write as

$$L^0_{j,j+1}(n) = L_{j,j+1} \cap \{\bigcup_{m=1}^{n-1} F^{n-m} L^0_{j-1,j}(m)\} \tag{A.2}$$

for $j \geq 1$. The R_0 particles which lie on C_j, $(j \geq 1)$ at iterate $n-1$ must pass through $L_{j-1,j}$ until $t = n-2$, so that we have

$$C_j \cap F^{n-1}C_0 = C_j \cap \{\bigcup_{m=1}^{n-1} F^{n-m} L^0_{j-1,j}(m)\} \tag{A.3}$$

for $j \geq 1$. For simplicity let us put

$$K_j(n) \equiv \bigcup_{m=1}^{n} F^{n-m+1} L^0_{j-1,j}(m). \tag{A.4}$$

Then (A.3) and (A.2) lead to

$$T_j(n-1) = \mu(C_j \cap K_j(n-1)), \tag{A.5}$$

$$\mu(L^0_{j,j+1}(n)) = \mu(L_{j,j+1} \cap K_j(n-1)). \tag{A.6}$$

Since $n \gg j\tau_B + 1$, the R_0 particles are sufficiently mixed in each C_j so that their spatial distribution within C_j is nearly uniform except a few lobes

such as $FL_{j\mp1,j}$ and their particle concentration $T_j(n)$ is slowly varying in j. Then the initial memory of the R_0 particles is lost in $K_j(n-1)$ so that $\mu(L^0_{j,j+1}(n))$ is locally determined by $T_j(n-1)$, leading to the local relation

$$\mu(L^0_{j,j+1}(n)) = \eta T_j(n-1) \tag{A.7}$$

with $\eta \equiv \mu(L_{j,j+1})/\mu(C_j) = \mu(L_{0,1})/\mu(C_0)$. This relation means that the amount of the R_0 particles which enter C_{j+1} at iterate n by passing through $L_{j,j+1}$ at iterate $n-1$ is proportional to their particle concentration of C_j at iterate $n-1$, and its transfer rate is given by the ratio η. This is physically reasonable. Inserting (A.7) into the left-hand side of (A.1), we obtain $D = \eta = \mu(L_{0,1})/\mu(C_0)$ which is the relation proposed for D.

References

[1] H. Poincaré, *Les Methods Nouvelles de la Mechanique Celeste*, (Gauthier-Villars, Paris, 1892)

[2] E. N. Lorentz, J. Atmos. Sci. **20**(1963), 130

[3] D. Ruelle and F. Takens, Commun. Math. Phys. **20**(1971), 167

[4] S. Smale, *Differential and Combinatorial Topology*, (Princeton University Press, Princeton, 1963)

[5] L. D. Landau and E. M. Lifshitz, *Fluid Mechanics 2nd edition*, (Pergamon Press, 1984)

[6] H. Aref, J. Fluid Mech. **143**(1984), 1.
J. Chaiken, R. Chevray, M. Tabor and Q. M. Tan, Proc. R. Soc. London **A408**(1986), 165.

[7] D. S. Broomhead and S. C. Ryrie, Nonlinearity **1**(1988), 409

[8] J. G. Franjino, C. W. Leong and J. M. Ottino, Phys. Fuids **A1**(1989), 1772.
J. M. Ottino, *The Kinematics of Mixing*, (Cambridge University Press, New York, 1989).

[9] R. Iwatsu, K. Ishii, T. Kawamura, K. Kawahara Fluid Nyn. Res. **5**(1989), 173

[10] M. Falcioni, G. Paladin and A. Vulpiani J. Phys. **A21**(1988), 3451

[11] F. H. Busse Rep. Prog. Phys. **41**(1978), 1929

[12] J. Hale *Ordinary Differential Equations*, (Co., Inc.: Malabar, Florida, 1980)

[13] M. W. Hirsh and S. Smale, *Differential Equations, Dynamical Systems and Linear Algebra*, (Academic Press, New York, 1974)

[14] C. Nash and S. Sen, *topology and Geometry for Physics*, (Academic Press, New York, 1983)

[15] R. W. Easton Trans. Amer. Math. Soc. **294**(1986), 714

[16] S. R. Channon and J. L. Lebowitz, Ann. New York Akad. Sci. **357**(1980), 108

[17] J. H. Bartlett, Celestial Mech. **28**(1982), 295

[18] V. I. Arnold and A. Avez *Ergodic Problems of Classical Mechanics*, (Benjamin, New York, 1968)

[19] R. M. Clever and F. H. Busse, J. Fluid Mech. **65**(1975), 625

[20] T. H. Solomon and J. P. Gollub, Phys. Rev. **A38**(1988), 6280.

[21] K. Ouchi, N. Mori, T. Horita and H. Mori, Prog. Theor. Phys. **85**(1991), 687.

[22] K. Ouchi and H. Mori Prog. Theor. Phys. **88**(1992), 457

[23] H. Mori, H. Hata, T. Horita and T. Kobayashi, Prog. Thero. Phys. Suppl. **No.99**(1989), 1.

[24] R. Ishizaki, T. Hata, T. Horita and H. Mori, Prog. Theor. Phys. **84**(1990), 179.

[25] R. Ishizaki, T. Horita, T. Kobayashi and H. Mori, Prog. Theor. Phys. **85**(1991), 1013.

[26] S. Wiggins, *Introduction to Applied Nonlinear Dynamical Systems and Chaos*, (Springer-Verlag, New York, 1990), §4.6.
S. Wiggins, Chaotic Transport in Dynamical Systems **Springer-Verlag**(19New York), 1992, Sec.3.2.

[27] R. Camassa and S. Wiggins, Phys. Rev. **A43**(1991), 774.

[28] S. Chandrasekhar, *Hydrodynamic and Hydromagnetic Stability*, (Dover, New York, 1961).

[29] A. J. Lichtenberg and M.A. Lieberman, *Regular and Stochastic Motion*, (Springer-Verlag, New Yorkf, 1982).
R.S. Mackay and J.D. Meiss, *Hamiltonian Dynamical Systems*, (Adam Higler, Bristol, 1987).

[30] J. Guckenheimer and P.Holmes, *Nonlinear Oscillations, Dynamical Systems, and Bifurcations of Vector Fields*, (Springer-Verlag, New York, 1983).

[31] J. M. Greene, R. S. Mackay, F. Vivaldi and M. J. Feigenbaum, Physica **3D**(1981), 468.

[32] Y. H. Ichikawa, T. Kamimura and T. Hatori, Physica **29D**(1987), 247.

[33] C. F. F. Karney, Physica **8D**(1983), 360.

[34] T. Horita, H. Hata, R. Ishizakiand H. Mori, Prog. Theor. Phys. **83**(1990), 1065.
Rom-Keder, A. Leonard and S. Wiggins, J. Fluid Mech. **214**(1990), 347.

[35] R. S. Mackay, J. D. Meiss and I. C. Percival, Physica **13D**(1984), 55.

[36] V. Rom-Keder and S. Wiggins, Arch. Ration. Mech. Anal. **109**(1990), 239.

[37] W. Feller, Trans. Am. Math. Soc. **67**(1949), 98.

[38] T. Horita and H. Mori, in *From Phase Transition to Chaos*, edited by Gyorgi et al (World Scientific, Singapore,1992).

[39] X. -J. Wang, Phys. Rev. **A40**(1989), 6647.

[40] E. Moses and V. Steinberg, Physica **D37**(1989), 341.

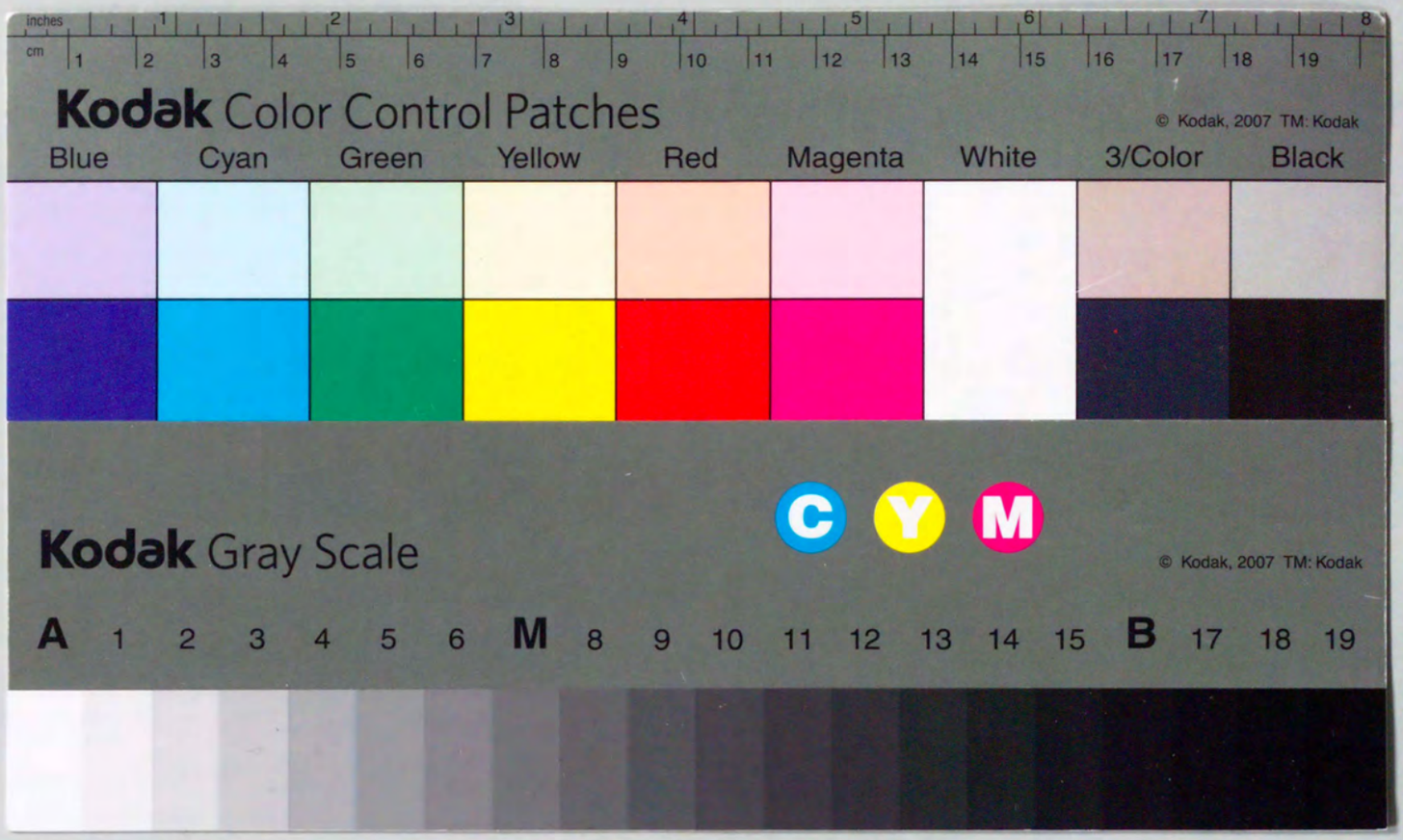
inches
cm
Kodak Color Control Patches
© Kodak, 2007 TM: Kodak
Blue
Cyan
Green
Yellow
Red
Magenta
White
3/Color
Black
Kodak Gray Scale
C
Y
M
© Kodak, 2007 TM: Kodak
A 1 2 3 4 5 6 M 8 9 10 11 12 13 14 15 B 17 18 19